

Efficiency, Curvature, and Complexity of Quantum Evolutions for Qubits in Nonstationary Magnetic Fields

Carlo Cafaro¹ and James Schneeloch^{21,2}

¹¹University at Albany-SUNY, Albany, NY 12222, USA

²²Air Force Research Laboratory, Information Directorate, Rome, New York, 13441, USA

In optimal quantum-mechanical evolutions, motion can take place along paths of minimal length within an optimal time frame. Alternatively, optimal evolutions may occur along established paths without any waste of energy resources and achieving 100% speed efficiency. Unfortunately, realistic physical scenarios often lead to less-than-ideal evolutions that demonstrate suboptimal efficiency, nonzero curvature, and a high level of complexity.

In this paper, we provide an exact analytical expression for the curvature of a quantum evolution pertaining to a two-level quantum system subjected to various time-dependent magnetic fields. Specifically, we examine the dynamics produced by a two-parameter nonstationary Hermitian Hamiltonian with unit speed efficiency. To enhance our understanding of the physical implications of the curvature coefficient, we analyze the curvature behavior in relation to geodesic efficiency, speed efficiency, and the complexity of the quantum evolution (as described by the ratio of the difference between accessible and accessed Bloch-sphere volumes for the evolution from initial to final state to the accessible volume for the given quantum evolution). Our findings indicate that, generally, efficient quantum evolutions exhibit lower complexity compared to inefficient ones. However, we also note that complexity transcends mere length. In fact, longer paths that are sufficiently curved can demonstrate a complexity that is less than that of shorter paths with a lower curvature coefficient.

PACS numbers: Complexity (89.70.Eg), Quantum Computation (03.67.Lx), Quantum Information (03.67.Ac), Quantum Mechanics (03.65.-w), Riemannian Geometry (02.40.Ky).

I. INTRODUCTION

It is recognized that geometric reasoning can provide significant insights in the realm of quantum physics [1]. For example, when concentrating on pure states, we can pinpoint Hamiltonian operators that facilitate quantum evolutions at the maximum achievable rate [2–8]. These quantum dynamical trajectories, referred to as Hamiltonian curves, adhere to geodesic paths on the metricized manifolds of quantum states, as the states progress according to defined physical evolutions. A key quantity employed to measure the deviation from the ideal geodesic evolution on a manifold of pure states is the so-called geodesic efficiency η_{GE} , which was introduced by Anandan and Aharonov in Ref. [9]. This quantity serves as a global measure since it is assessed over a finite time interval. It is articulated in terms of the ratio between two lengths, s_0 and s . The length s_0 represents the geodesic distance, which is the length of the shortest path connecting the initial and final states ($|A\rangle$ and $|B\rangle$, respectively) as measured with respect to the Fubini-Study metric (where $s_0 = 2s_{FS}$, with s_{FS} denoting the Fubini-Study distance). Conversely, the length s characterizes the actual path traversed by the quantum system. Specifically, s is influenced by the energy uncertainty of the system, which is governed by either a stationary or a time-varying Hamiltonian.

In geometric quantum mechanics, the analysis of parameter estimation introduces the concept of curvature of a quantum Schrödinger trajectory, as presented in Ref. [10]. This concept serves as a generalization of the curvature notion found in classical exponential families of distributions utilized in statistical mechanics. In Ref. [10], the curvature of a curve is defined through a suitably introduced squared acceleration vector associated with the curve. Moreover, this curvature quantifies the parametric sensitivity relevant to the parametric estimation problem under investigation [11]. In Ref. [12], Laba and Tkachuk established definitions for curvature and torsion coefficients pertaining to quantum evolutions of pure states that undergo time-independent Hamiltonian evolution. In particular, by concentrating on single-qubit quantum states, they demonstrated that curvature serves as a measure of how much the dynamically evolving state vector deviates from the geodesic line on the Bloch sphere. Utilizing the Frenet-Serret apparatus concept and partially drawing from the research conducted by Laba and Tkachuk as referenced in [12], an alternative geometric framework to define the bending and twisting of quantum curves represented by dynamically evolving state vectors within a quantum context was introduced in Refs. [13–15]. In particular, it was proposed a quantum adaptation of the Frenet-Serret apparatus for a quantum trajectory in projective Hilbert space, which is delineated by a parallel-transported pure quantum state that evolves unitarily under a stationary (or, alternatively, nonstationary) Hamiltonian that governs the Schrödinger equation. In the case of nonstationary Hamiltonian evolutions, the authors reported in Ref. [14] that the time-varying framework revealed a more intricate structure from a statistical perspective compared to the stationary framework [13]. To effectively demonstrate the

relevance of their construct, the authors applied it to an exactly solvable time-dependent two-state Rabi problem characterized by a sinusoidal oscillating time-dependent potential. Within this framework, they illustrated that the analytical formulations for the curvature and torsion coefficients can, in principle, be entirely described using only two real three-dimensional vectors: the Bloch vector that defines the quantum system and the externally applied time-varying magnetic field. Although they established that the torsion is identically zero for any arbitrary time-dependent single-qubit Hamiltonian evolution, they only examined the temporal behavior of the curvature coefficient numerically across various dynamical scenarios, including both off-resonance and on-resonance conditions, as well as strong and weak driving configurations. In Ref. [16], the first exact analytical analysis of the curvature of the trajectory of a two-level quantum system subjected to a time-varying magnetic field was recorded in the literature. Nonetheless, only one temporal profile of the magnetic field was examined.

The importance of the concepts of length and volume is vital in establishing complexity within a quantum mechanical context. In the field of quantum physics, there are numerous interpretations of complexity. For instance, one might refer to the complexity linked to a quantum state (state complexity, [17, 18]), the complexity present in a quantum circuit (circuit complexity, [19, 20]), or the complexity associated with an operator (operator complexity, [21–24]). Although these measures of complexity possess unique attributes, they are united by a fundamental principle: the complexity of a composite system generally escalates in relation to the number of essential components needed for its assembly [25–27]. Depending on the situation, this correlation can frequently be expressed through geometrically intuitive concepts such as lengths and volumes. In the area of theoretical computer science, Kolmogorov asserted in Ref. [28] that the complexity of a sequence can be measured by the length of the shortest Turing machine program that can produce it. Furthermore, in the sphere of information theory, Rissanen proposed in Refs. [29, 30] that the average minimal code length of a collection of messages acts as an indicator of the complexity of that collection.

Returning to the geometric quantifiers of complexity, state complexity pertains to the intricacy of a quantum state, defined in terms of the minimal local unitary circuit that can generate the state from a fundamental (i.e., factorizable) reference quantum state. Notably, a geometric perspective on state complexity was first introduced during the investigation of quantum state complexity in continuous many-body systems. Specifically, the state complexity of a target state, obtained by applying a sequence of parametrized unitary operators to a source state, was depicted as the length of the shortest path, as determined by the Fubini-Study metric, that corresponds to a valid realization of the unitary operator [17]. Quantum circuits are composed of quantum gates that act on quantum states. In particular, circuit complexity refers to the minimum number of primitive gates necessary to create a circuit that executes a transformation on a designated quantum state [19, 20]. This complexity is fundamentally discrete and serves as an important metric for researchers involved in the practical development of quantum circuits from basic gates. Importantly, the notions of state complexity and circuit complexity are interrelated; state complexity relates to the least complex unitary operator that connects the source and target states. The geometric characterization of circuit complexity was proposed by Nielsen and his associates in Refs. [31–33]. Within this geometric framework, the circuit complexity linked to a unitary operator U is inherently continuous and corresponds to the length of the shortest geodesic that connects the identity operator to U within the unitary group. The lengths of these geodesic paths act as a lower limit for the minimum number of quantum gates necessary to create the unitary operator U . Additionally, operator complexity relates to the temporal growth in the size of an operator as it progresses under the Heisenberg or Lindblad dynamics for closed and open quantum systems, respectively. When evaluated in the context of the Krylov basis, this operator complexity is termed Krylov complexity [21]. For completeness, we remark that the size of an evolving operator is measured by the average size of the basis operators in its expansion. Basis operators are simple local operators such as single-site Pauli operators on a spin-chain and, in addition, their size is specified by the number of sites on which they act nontrivially. In Ref. [24], the time evolution of the displacement operator during the unitary evolution of many-body quantum systems characterized by symmetries demonstrated that the expectation value of the Krylov complexity operator is equivalent to the volume of the corresponding classical phase space. The connection between Krylov complexity and volume was further investigated within particular quantum field theoretic frameworks. Importantly, the scaling of this complexity with volume was validated in Ref. [22] by illustrating that Krylov complexity is associated with the average particle number. This connection was effectively justified by utilizing the proportionality between volume and average particle number.

In Refs. [34, 35], an alternative measure of complexity was introduced for examining the complexities of both time-optimal and time sub-optimal quantum Hamiltonian evolutions that connect arbitrary source and target states on the Bloch sphere, utilizing the Fubini-Study metric. The notion of complexity was articulated in terms of the accessed (i.e., partial) and accessible (i.e., total) parametric volumes of the areas on the Bloch sphere that delineate the quantum mechanical evolution from the source to the target states. Specifically, by concentrating on time optimal and time suboptimal evolutions, the characteristics of complexity were juxtaposed with those of path length, geodesic efficiency, and the curvature coefficient that define the evolutions. Generally, it was determined that efficient quantum evolutions exhibit lower complexity compared to inefficient ones. Nevertheless, the authors also noted in Refs. [34, 35] that complexity transcends mere length. In fact, longer paths that are sufficiently curved can demonstrate a complexity

that is less than that of shorter paths with a lower curvature coefficient. However, the analysis was confined to stationary Hamiltonian evolutions.

Driven by the lack of research on the geometric characterization of nonstationary Hamiltonian evolutions in two-level quantum systems, particularly regarding efficiency, curvature, and complexity, this paper seeks to fill this gap by addressing fundamental questions, including:

- [i] The analytical solution of Schrödinger's evolution equation for two-level systems in the presence of time-dependent magnetic field configurations can be quite complex. Is it possible to identify a category of time-varying magnetic field configurations for which precise analytical solutions can be derived?
- [ii] Relative phases hold physical significance, exhibiting observable effects in quantum mechanics. Can we establish a general method to connect these relative phases to specific magnetic field configurations that define the nonstationary Hamiltonians of interest?
- [iii] Having established the relationship between generally time-varying phases and magnetic field configurations, can we measure the impact of their appropriately chosen temporal behavior on the path lengths, energy dissipation, and degree of trajectory curvature when examining the quantum evolution between fixed initial and final states on the Bloch sphere?
- [iv] With a clear understanding of how relative phases and magnetic field configurations influence these geometric characteristics of quantum dynamical trajectories (i.e., geodesic efficiency, speed efficiency, and curvature coefficient), can we grasp how they affect the complexity of the dynamical evolutions in terms of the accessed and accessible volumes of parametric regions of the Bloch sphere?

Addressing these issues is significant for various reasons within the domain of quantum information and computation. For example, a thorough quantitative comprehension of these matters can assist in the development of appropriate time-dependent quantum driving strategies that are capable of transferring a source state to a target state in the least amount of time, at optimal speed, with minimal energy resource waste, and ultimately, with reduced complexity.

The layout of the rest of this paper is as follows. In Section II, we present the fundamental components necessary for comprehending the concepts of geodesic efficiency and speed efficiency [36] in quantum-mechanical evolutions. In Section III, we advance to the characterization of the geometric features of quantum evolutions by introducing the notions of curvature coefficient and the complexity of dynamical trajectories traced by state vectors, whose dynamics are dictated by nonstationary Hamiltonians. In Section IV, we introduce a two-parameter family of time-varying Hamiltonians, which we aim to analyze geometrically. Specifically, we concentrate on the time-dependent configurations of the magnetic fields that define the Hamiltonians, as well as the temporal behavior of the phase that determines the relative phase factor involved in the decomposition of the evolving state in terms of the computational basis state vectors. In Section V, we utilize the concepts introduced in Sections II and III to characterize the quantum evolutions discussed in Section IV. In particular, by focusing on the temporal dependence of the aforementioned phase, we examine five distinct scenarios: i) no growth; ii) linear growth; iii) quadratic growth; iv) exponential growth; v) exponential decay. Our summary of findings, along with our concluding remarks, can be found in Section V. Finally, technical details appear in Appendix A.

II. EFFICIENCY

In this section, we outline the essential elements required to understand the principles of geodesic efficiency and speed efficiency in quantum-mechanical evolutions.

A. Geodesic Efficiency

Consider the evolution of a state vector $|\psi(t)\rangle$ as described by the time-dependent Schrödinger equation, $i\hbar\partial_t|\psi(t)\rangle = H(t)|\psi(t)\rangle$, within the interval $t_A \leq t \leq t_B$. Consequently, the geodesic efficiency η_{GE} for this quantum evolution is a scalar quantity that remains constant over time (global) and is defined within the range of $0 \leq \eta_{GE} \leq 1$. It equals [9, 37]

$$\eta_{GE} \stackrel{\text{def}}{=} \frac{s_0}{s} = \frac{2 \arccos [|\langle A|B\rangle|]}{2 \int_{t_A}^{t_B} \frac{\Delta E(t)}{\hbar} dt}. \quad (1)$$

The quantity s_0 represents the distance along the shortest geodesic path connecting the initial state $|A\rangle \stackrel{\text{def}}{=} |\psi(t_A)\rangle$ and the final state $|B\rangle \stackrel{\text{def}}{=} |\psi(t_B)\rangle$ within the complex projective Hilbert space. Moreover, the quantity s in Eq. (1) signifies the distance along the dynamical trajectory $\gamma(t) : t \mapsto |\psi(t)\rangle$ that corresponds to the evolution of the state vector $|\psi(t)\rangle$ for $t_A \leq t \leq t_B$. Clearly, a geodesic quantum evolution characterized by $\gamma(t) = \gamma_{\text{geo}}(t)$ is established through the equation $\eta_{\text{GE}}^{(\gamma_{\text{geo}})} = 1$. By concentrating on the numerator in Eq. (1), we observe that it specifies the angle between the unit state vectors $|A\rangle$ and $|B\rangle$, which is equivalent to the Wootters distance [38]. Specifically, we define $\rho_A \stackrel{\text{def}}{=} |A\rangle\langle A| = (\mathbf{1} + \mathbf{a} \cdot \boldsymbol{\sigma})/2$ and $\rho_B \stackrel{\text{def}}{=} |B\rangle\langle B| = (\mathbf{1} + \mathbf{b} \cdot \boldsymbol{\sigma})/2$, where \mathbf{a} and \mathbf{b} are unit vectors such that $\mathbf{a} \cdot \mathbf{b} = \cos(\theta_{AB})$. Consequently, it follows that $s_0 = \theta_{AB}$, given that $|\langle A|B\rangle|^2 = \text{tr}(\rho_A \rho_B) + 2\sqrt{\det(\rho_A) \det(\rho_B)} = (1 + \mathbf{a} \cdot \mathbf{b})/2 = \cos^2(\theta_{AB}/2)$. Evidently, $\boldsymbol{\sigma} \stackrel{\text{def}}{=} (\sigma_x, \sigma_y, \sigma_z)$ represents the vector operator defined by the standard Pauli operators. Conversely, the denominator in Eq. (1) denotes the integral of the infinitesimal distance $ds \stackrel{\text{def}}{=} 2[\Delta E(t)/\hbar]dt$ along the evolution curve in ray space [9]. The term $\Delta E(t) \stackrel{\text{def}}{=} [\langle\psi|H^2(t)|\psi\rangle - \langle\psi|H(t)|\psi\rangle^2]^{1/2}$ signifies the energy uncertainty of the system, articulated as the square root of the dispersion of $H(t)$. Significantly, Anandan and Aharonov demonstrated that the infinitesimal distance $ds \stackrel{\text{def}}{=} 2[\Delta E(t)/\hbar]dt$ is related to the Fubini-Study infinitesimal distance ds_{FS} through the relationship [9],

$$ds_{\text{FS}}^2 (|\psi(t)\rangle, |\psi(t+dt)\rangle) \stackrel{\text{def}}{=} 4 \left[1 - |\langle\psi(t)|\psi(t+dt)\rangle|^2 \right] = 4 \frac{\Delta E^2(t)}{\hbar^2} dt^2 + \mathcal{O}(dt^3), \quad (2)$$

where $\mathcal{O}(dt^3)$ denotes an infinitesimal quantity of an order that is equal to or greater than dt^3 . From the relationship between ds_{FS} and ds , it can be concluded that s is proportional to the time integral of ΔE . Furthermore, s represents the distance calculated by the Fubini-Study metric throughout the evolution of the quantum system in ray space. It is important to emphasize that when the actual dynamical curve corresponds to the shortest geodesic path connecting $|A\rangle$ and $|B\rangle$, s is equal to s_0 , and the geodesic efficiency η_{GE} in Eq. (1) equals one. Evidently, π represents the minimal distance between two orthogonal pure states within ray space. Notably, we observe that by defining $H(t) \stackrel{\text{def}}{=} h_0(t) \mathbf{1} + \mathbf{h}(t) \cdot \boldsymbol{\sigma}$ and $\rho(t) \stackrel{\text{def}}{=} (\mathbf{1} + \mathbf{a}(t) \cdot \boldsymbol{\sigma})/2$ for $t_A \leq t \leq t_B$, the energy uncertainty simplifies to $\Delta E(t) = \sqrt{\mathbf{h}^2 - [\mathbf{a}(t) \cdot \mathbf{h}]^2}$. Ultimately, the geodesic efficiency expressed in Eq. (1) can be reformulated as

$$\eta_{\text{GE}} = \frac{2 \arccos \left(\sqrt{\frac{1+\mathbf{a} \cdot \mathbf{b}}{2}} \right)}{\int_{t_A}^{t_B} \frac{2}{\hbar} \sqrt{\mathbf{h}^2 - [\mathbf{a}(t) \cdot \mathbf{h}]^2} dt}, \quad (3)$$

where $\mathbf{a}(t_A) \stackrel{\text{def}}{=} \mathbf{a}$ and $\mathbf{a}(t_B) = \mathbf{b}$ in Eq. (3). Intriguingly, assuming $H(t) \stackrel{\text{def}}{=} \mathbf{h}(t) \cdot \boldsymbol{\sigma}$ and putting $\mathbf{h} = [\mathbf{h} \cdot \mathbf{a}] \mathbf{a} + [\mathbf{h} - (\mathbf{h} \cdot \mathbf{a}) \mathbf{a}] = \mathbf{h}_{\parallel} + \mathbf{h}_{\perp}$ (where, of course, $\mathbf{a} = \mathbf{a}(t)$ in the decomposition of \mathbf{h}), the geodesic efficiency η_{GE} in Eq. (3) becomes (setting $\hbar = 1$, which results in \mathbf{h} being expressed not in units of energy, but rather in units of frequency)

$$\eta_{\text{GE}} = \frac{\arccos \left(\sqrt{\frac{1+\mathbf{a} \cdot \mathbf{b}}{2}} \right)}{\int_{t_A}^{t_B} h_{\perp}(t) dt}. \quad (4)$$

Consequently, from Eq. (4), it is evident that η_{GE} is solely dependent on $h_{\perp}(t)$. Interestingly, by maintaining $\hbar = 1$, we observe that Feynman's geometric evolution equation [1] $d\mathbf{a}/dt = 2\mathbf{h} \times \mathbf{a}$, which pertains to the time-dependent unit Bloch vector $\mathbf{a} = \mathbf{a}(t)$, can be interpreted as a local expression of the Anandan-Aharanov relation $s = 2 \int \Delta E(t) dt$. In fact, from $d\mathbf{a}/dt = 2\mathbf{h} \times \mathbf{a}$, we derive $da^2 = d\mathbf{a} \cdot d\mathbf{a} = 4h_{\perp}^2 dt^2$. Likewise, from $s = 2 \int \Delta E(t) dt$, we can deduce $ds = 2h_{\perp} dt$. Thus, by merging these two differential equations, we ultimately arrive at $da = \sqrt{d\mathbf{a} \cdot d\mathbf{a}} = 2h_{\perp} dt = ds$.

After this concise overview of geodesic efficiency, we are now prepared to introduce the notion of speed efficiency.

B. Speed Efficiency

Suitable families of nonstationary Hamiltonians that can produce predetermined dynamical trajectories with minimal energy resource waste were originally introduced in Ref. [36]. While these trajectories are efficient in terms of energy, they do not typically represent geodesic paths of the shortest length. The condition for minimal energy waste is achieved when no energy is expended on segments of the Hamiltonian $H = H(t)$ that do not effectively guide the

system. In other words, all the energy available, as indicated by the spectral norm of the Hamiltonian $\|H\|_{\text{SP}}$, is converted into the system's evolution speed $v_H(t) \stackrel{\text{def}}{=} (2/\hbar)\Delta E(t)$, where $\Delta E(t)$ denotes the energy uncertainty. More explicitly, Uzdin's speed efficiency η_{SE} refers to a time-dependent (local) scalar quantity that satisfies the condition $0 \leq \eta_{\text{SE}} \leq 1$. It is defined as

$$\eta_{\text{SE}}(t) \stackrel{\text{def}}{=} \frac{\Delta H_\rho}{\|H\|_{\text{SP}}} = \frac{\sqrt{\text{tr}(\rho H^2) - [\text{tr}(\rho H)]^2}}{\max[\sqrt{\text{eig}(H^\dagger H)}]}. \quad (5)$$

While $\Delta H_\rho = \Delta E(t)$ and $\rho = \rho(t)$ represents the density operator that characterizes the quantum system at time t , the term $\|H\|_{\text{SP}}$ found in the denominator of Eq. (5) is defined as $\|H\|_{\text{SP}} \stackrel{\text{def}}{=} \max[\sqrt{\text{eig}(H^\dagger H)}]$. This term is known as the spectral norm $\|H\|_{\text{SP}}$ of the Hamiltonian operator H , serving as a measure of the magnitude of bounded linear operators. It is calculated as the square root of the maximum eigenvalue of the operator $H^\dagger H$, where H^\dagger signifies the Hermitian conjugate of H . Concentrating on two-level quantum systems and presuming the nonstationary Hamiltonian in Eq. (5) is represented by $H(t) \stackrel{\text{def}}{=} h_0(t) \mathbf{1} + \mathbf{h}(t) \cdot \boldsymbol{\sigma}$, we find that the speed efficiency η_{SE} in Eq. (5) can be effectively articulated as

$$\eta_{\text{SE}}(t) \stackrel{\text{def}}{=} \frac{\sqrt{\mathbf{h}^2 - (\mathbf{a} \cdot \mathbf{h})^2}}{|h_0| + \sqrt{\mathbf{h}^2}}. \quad (6)$$

While $\mathbf{a} = \mathbf{a}(t)$ in Eq. (6) represents the instantaneous unit Bloch vector characterizing the qubit state of the system, the set $\text{eig}(H^\dagger H)$ in the definition of $\|H\|_{\text{SP}}$ is equivalent to $\text{eig}(H^\dagger H) = \{\lambda_{H^\dagger H}^{(+)} \stackrel{\text{def}}{=} (h_0 + \sqrt{\mathbf{h}^2})^2, \lambda_{H^\dagger H}^{(-)} \stackrel{\text{def}}{=} (h_0 - \sqrt{\mathbf{h}^2})^2\}$. It is important to note that the eigenvalues of $H(t) \stackrel{\text{def}}{=} h_0(t) \mathbf{1} + \mathbf{h}(t) \cdot \boldsymbol{\sigma}$ are given by $E_\pm \stackrel{\text{def}}{=} h_0 \pm \sqrt{\mathbf{h} \cdot \mathbf{h}}$. Consequently, the term $h_0 = (E_+ + E_-)/2$ signifies the mean value of the two energy levels. Moreover, $\sqrt{\mathbf{h}^2} = (E_+ - E_-)/2$ is directly proportional to the energy difference $E_+ - E_-$ between the two energy states E_\pm , where E_+ is greater than or equal to E_- . Lastly, for a time-dependent Hamiltonian $H(t) \stackrel{\text{def}}{=} \mathbf{h}(t) \cdot \boldsymbol{\sigma}$ that satisfies $\mathbf{a}(t) \cdot \mathbf{h}(t) = 0$ at every moment in time t , the speed efficiency $\eta_{\text{SE}}(t)$ equals one. Consequently, quantum evolution for a time-dependent Hamiltonian with stationary eigenvalues occurs without any depletion of energy resources. Notably, for $H(t) \stackrel{\text{def}}{=} \mathbf{h}(t) \cdot \boldsymbol{\sigma}$ and by defining $\mathbf{h} = (\mathbf{h} \cdot \mathbf{a})\mathbf{a} + [\mathbf{h} - (\mathbf{h} \cdot \mathbf{a})\mathbf{a}] = \mathbf{h}_{||} + \mathbf{h}_\perp$ with $\mathbf{h}_{||} \cdot \mathbf{h}_\perp = 0$, $\eta_{\text{SE}}(t)$ in Eq. (6) can be entirely represented by means of the parallel (i.e., $\mathbf{h}_{||} \stackrel{\text{def}}{=} h_{||}\hat{h}_{||}$) and transverse (i.e., $\mathbf{h}_\perp \stackrel{\text{def}}{=} h_\perp\hat{h}_\perp$) components of the magnetic field vector \mathbf{h} as

$$\eta_{\text{SE}}(t) = \frac{h_\perp(t)}{\sqrt{h_\perp^2(t) + h_{||}^2(t)}}. \quad (7)$$

From Eq. (7), it is clear that $\eta_{\text{SE}}(t) = 1$ if and only if $h_{||}(t) = 0$ for all t . In other terms, this condition holds true if and only if the orthogonality condition $\mathbf{a}(t) \cdot \mathbf{h}(t) = 0$ is fulfilled for every t .

After this concise overview of geodesic and speed efficiencies, we are now ready to present the concepts of curvature and the complexity associated with quantum evolutions.

III. CURVATURE AND COMPLEXITY

In this section, we will characterize the geometric properties of quantum evolutions by introducing the concepts of curvature coefficient and the complexity of the dynamical paths taken by state vectors, which are governed by nonstationary Hamiltonians.

A. Curvature

We commence with the notion of the curvature coefficient in quantum evolution. Following a few mathematical details and a formal definition, we concentrate on the explicit computation of this coefficient for both higher-dimensional systems and two-level systems.

1. Preliminaries

In the broadest sense, consider a nonstationary Hamiltonian evolution characterized by Schrödinger's equation $i\hbar\partial_t|\psi(t)\rangle = H(t)|\psi(t)\rangle$, where $|\psi(t)\rangle$ is an element of an arbitrary N -dimensional complex Hilbert space \mathcal{H}_N . Generally, the normalized state vector $|\psi(t)\rangle$ satisfies the condition $\langle\psi(t)|\dot{\psi}(t)\rangle = (-i/\hbar)\langle\psi(t)|H(t)|\psi(t)\rangle \neq 0$. For the state $|\psi(t)\rangle$, we define the parallel transported unit state vector $|\Psi(t)\rangle \stackrel{\text{def}}{=} e^{i\beta(t)}|\psi(t)\rangle$ where the phase $\beta(t)$ is determined such that $\langle\Psi(t)|\dot{\Psi}(t)\rangle = 0$. Note that $i\hbar\langle\Psi(t)|\dot{\Psi}(t)\rangle = [H(t) - \hbar\dot{\beta}(t)]|\Psi(t)\rangle$. Consequently, the relation $\langle\Psi(t)|\dot{\Psi}(t)\rangle = 0$ is equivalent to setting $\beta(t) \stackrel{\text{def}}{=} (1/\hbar)\int_0^t \langle\psi(t')|H(t')|\psi(t')\rangle dt'$. For this reason, $|\Psi(t)\rangle$ simplifies to

$$|\Psi(t)\rangle = e^{(i/\hbar)\int_0^t \langle\psi(t')|H(t')|\psi(t')\rangle dt'}|\psi(t)\rangle, \quad (8)$$

and fulfills the evolution equation $i\hbar\langle\dot{\Psi}(t)\rangle = \Delta H(t)|\Psi(t)\rangle$ with $\Delta H(t) \stackrel{\text{def}}{=} H(t) - \langle H(t)\rangle$. Note that the speed $v(t)$ of quantum evolution varies when the Hamiltonian is time-varying. Specifically, $v(t)$ is defined such that $v^2(t) = \langle\dot{\Psi}(t)|\dot{\Psi}(t)\rangle = \langle(\Delta H(t))^2\rangle/\hbar^2$. For convenience, we define the arc length $s = s(t)$ in terms of $v(t)$ as $s(t) \stackrel{\text{def}}{=} \int_0^t v(t')dt'$, with $ds = v(t)dt$ (which, in turn, implies that $\partial_t = v(t)\partial_s$). Evidently, $\partial_t \stackrel{\text{def}}{=} \partial/\partial t$ and $\partial_s \stackrel{\text{def}}{=} \partial/\partial s$. In conclusion, by presenting the dimensionless operator

$$\Delta h(t) \stackrel{\text{def}}{=} \frac{\Delta H(t)}{\hbar v(t)} = \frac{\Delta H(t)}{\sqrt{\langle(\Delta H(t))^2\rangle}}, \quad (9)$$

the normalized tangent vector $|T(s)\rangle \stackrel{\text{def}}{=} \partial_s|\Psi(s)\rangle = |\Psi'(s)\rangle$ transforms into $|T(s)\rangle = -i\Delta h(s)|\Psi(s)\rangle$. It is noted that $\langle T(s)|T(s)\rangle = 1$ by design, and furthermore, $\partial_s\langle\Delta h(s)\rangle = \langle\Delta h'(s)\rangle$. We can derive $|T'(s)\rangle \stackrel{\text{def}}{=} \partial_s|T(s)\rangle$ from the tangent vector $|T(s)\rangle = -i\Delta h(s)|\Psi(s)\rangle$. Indeed, through algebraic manipulation, we arrive at $|T'(s)\rangle = -i\Delta h(s)|\Psi'(s)\rangle - i\Delta h'(s)|\Psi(s)\rangle$ where $\langle T'(s)|T'(s)\rangle = \langle(\Delta h'(s))^2\rangle + \langle(\Delta h(s))^4\rangle - 2i\text{Re}\left[\langle\Delta h'(s)(\Delta h(s))^2\rangle\right] \neq 1$, in most cases. For clarity, we emphasize that the fourth power in $\langle(\Delta h(s))^4\rangle$ that appears in the expression for $\langle T'(s)|T'(s)\rangle$ originates from the relation $|\Psi'(s)\rangle = -i\Delta h(s)|\Psi(s)\rangle$. We are now ready to introduce the curvature coefficient for quantum evolutions produced by nonstationary Hamiltonians.

2. Definition

After introducing the vectors $|\Psi(s)\rangle$, $|T(s)\rangle$, and $|T'(s)\rangle$, we can now define the curvature coefficient as initially presented in Refs. [13–15], which is $\kappa_{\text{AC}}^2(s) \stackrel{\text{def}}{=} \langle\tilde{N}_*(s)|\tilde{N}_*(s)\rangle$. Observe that $|\tilde{N}_*(s)\rangle \stackrel{\text{def}}{=} P^{(\Psi)}|T'(s)\rangle$, where the projection operator $P^{(\Psi)}$ onto states that are orthogonal to $|\Psi(s)\rangle$ is defined as $P^{(\Psi)} \stackrel{\text{def}}{=} I - |\Psi(s)\rangle\langle\Psi(s)|$. Here, “I” represents the identity operator in \mathcal{H}_N . The subscript “AC” refers to Alsing and Cafaro. It is noteworthy that the curvature coefficient $\kappa_{\text{AC}}^2(s) = \langle\tilde{N}_*(s)|\tilde{N}_*(s)\rangle$ can be more conveniently expressed as

$$\kappa_{\text{AC}}^2(s) \stackrel{\text{def}}{=} \|D|T(s)\rangle\|^2 = \|D^2|\Psi(s)\rangle\|^2, \quad (10)$$

where $D \stackrel{\text{def}}{=} P^{(\Psi)}d/ds = (I - |\Psi\rangle\langle\Psi|)d/ds$ with $D|T(s)\rangle \stackrel{\text{def}}{=} P^{(\Psi)}|T'(s)\rangle = |\tilde{N}_*(s)\rangle$ denoting the covariant derivative [5, 39, 40]. According to Eq. (10), it is observed that the curvature coefficient $\kappa_{\text{AC}}^2(s)$ corresponds to the square of the magnitude of the second covariant derivative of the state vector $|\Psi(s)\rangle$ which defines the quantum Schrödinger trajectory within the framework of projective Hilbert space. To clarify, we highlight that $|\tilde{N}_*(s)\rangle$ is a vector that is neither orthogonal to the vector $|T(s)\rangle$ nor normalized to one. However, despite lacking proper normalization, $|\tilde{N}(s)\rangle \stackrel{\text{def}}{=} P^{(T)}P^{(\Psi)}|T'(s)\rangle$ is orthogonal to $|T(s)\rangle$. Ultimately, $|N(s)\rangle \stackrel{\text{def}}{=} |\tilde{N}(s)\rangle/\sqrt{\langle\tilde{N}(s)|\tilde{N}(s)\rangle}$ represents a normalized vector that is also orthogonal to $|T(s)\rangle$. In summary, the set $\{|\Psi(s)\rangle, |T(s)\rangle, |N(s)\rangle\}$ constitutes the three orthonormal vectors necessary for characterizing the curvature of a quantum evolution. It is important to note

that our focus is on the three-dimensional complex subspace spanned by $\{|\Psi(s)\rangle, |T(s)\rangle, |N(s)\rangle\}$, even though \mathcal{H}_N can possess an arbitrary dimension N as a complex space. Nonetheless, our selection aligns with the classical geometric viewpoint, where the curvature and torsion coefficients can be interpreted as the lowest and second-lowest members, respectively, of a family of generalized curvature functions [41].

3. Calculation technique: General case

The explicit computation of the time-dependent curvature coefficient $\kappa_{\text{AC}}^2(s)$ in Eqs. (10) utilizing the projection operators formalism often presents challenges. This difficulty arises because, akin to the classical scenario of space curves in \mathbb{R}^3 [42], there are fundamentally two issues encountered during the reparametrization of a quantum curve by its arc length s . Firstly, we may find it impossible to compute $s(t) \stackrel{\text{def}}{=} \int_0^t v(t')dt'$ in a closed form. Secondly, even if we succeed in determining $s = s(t)$, we might still face the challenge of inverting this relationship, thereby preventing us from obtaining $t = t(s)$, which is necessary to express $|\Psi(s)\rangle \stackrel{\text{def}}{=} |\Psi(t(s))\rangle$. To overcome these obstacles, we can reformulate $\kappa_{\text{AC}}^2(s)$ in Eq. (10) using expectation values calculated with respect to the state $|\Psi(t)\rangle$ (or, alternatively, with respect to $|\psi(t)\rangle$), which can be determined without relying on the relation $t = t(s)$ [13, 14]. For simplicity, we will not explicitly mention the s -dependence of the various operators and expectation values in the subsequent discussion. For instance, $\Delta h(s)$ will simply be denoted as Δh . After performing some algebraic manipulations, we arrive at $|\tilde{N}_*\rangle = -\left\{\left[(\Delta h)^2 - \langle(\Delta h)^2\rangle\right] + i[\Delta h' - \langle\Delta h'\rangle]\right\}|\Psi\rangle$, with $\Delta h' = \partial_s(\Delta h) = [\partial_t(\Delta h)]/v(t)$. To assess $\kappa_{\text{AC}}^2(s) \stackrel{\text{def}}{=} \langle\tilde{N}_*(s)|\tilde{N}_*(s)\rangle$, it is beneficial to introduce the Hermitian operator $\hat{\alpha}_1 \stackrel{\text{def}}{=} (\Delta h)^2 - \langle(\Delta h)^2\rangle$ along with the anti-Hermitian operator $\hat{\beta}_1 \stackrel{\text{def}}{=} i[\Delta h' - \langle\Delta h'\rangle]$, where it holds that $\hat{\beta}_1^\dagger = -\hat{\beta}_1$. Consequently, $|\tilde{N}_*\rangle = -(\hat{\alpha}_1 + \hat{\beta}_1)|\Psi\rangle$ and $\langle\tilde{N}_*(s)|\tilde{N}_*(s)\rangle$ is equivalent to $\langle\hat{\alpha}_1^2\rangle - \langle\hat{\beta}_1^2\rangle + \langle[\hat{\alpha}_1, \hat{\beta}_1]\rangle$, with $[\hat{\alpha}_1, \hat{\beta}_1] \stackrel{\text{def}}{=} \hat{\alpha}_1\hat{\beta}_1 - \hat{\beta}_1\hat{\alpha}_1$ representing the quantum commutator of $\hat{\alpha}_1$ and $\hat{\beta}_1$. It is important to note that the expectation value $\langle[\hat{\alpha}_1, \hat{\beta}_1]\rangle$ is a real number, as $[\hat{\alpha}_1, \hat{\beta}_1]$ represents a Hermitian operator. This arises from the nature of $\hat{\alpha}_1$ and $\hat{\beta}_1$ being Hermitian and anti-Hermitian operators, respectively. By applying the definitions of $\hat{\alpha}_1$ and $\hat{\beta}_1$, we derive $\langle\hat{\alpha}_1^2\rangle = \langle(\Delta h)^4\rangle - \langle(\Delta h)^2\rangle^2$, $\langle\hat{\beta}_1^2\rangle = -[\langle(\Delta h')^2\rangle - \langle\Delta h'\rangle^2]$, and $\langle[\hat{\alpha}_1, \hat{\beta}_1]\rangle = i\langle[(\Delta h)^2, \Delta h']\rangle$. It is noteworthy that, given that $[(\Delta h)^2, \Delta h']$ is an anti-Hermitian operator, $\langle[(\Delta h)^2, \Delta h']\rangle$ is purely imaginary. For thoroughness, we emphasize that $[(\Delta h)^2, \Delta h']$ is not typically a null operator. In fact, we have $[(\Delta h)^2, \Delta h'] = \Delta h[\Delta h, \Delta h'] + [\Delta h, \Delta h']\Delta h$ where $[\Delta h, \Delta h'] = [H, H']$. Consequently, when we focus for instance on nonstationary qubit Hamiltonians of the type $H(s) \stackrel{\text{def}}{=} \mathbf{h}(s) \cdot \boldsymbol{\sigma}$, the commutator $[H, H'] = 2i(\mathbf{h} \times \mathbf{h}') \cdot \boldsymbol{\sigma}$ may be nonzero, as the vectors \mathbf{h} and \mathbf{h}' are generally not collinear. Ultimately, a computationally efficient expression for the curvature coefficient $\kappa_{\text{AC}}^2(s)$ in Eq. (10) within any arbitrary nonstationary context simplifies to

$$\kappa_{\text{AC}}^2(s) = \langle(\Delta h)^4\rangle - \langle(\Delta h)^2\rangle^2 + \left[\langle(\Delta h')^2\rangle - \langle\Delta h'\rangle^2\right] + i\langle[(\Delta h)^2, \Delta h']\rangle. \quad (11)$$

From Eq. (11), it is observed that when the Hamiltonian H remains constant, $\Delta h'$ transforms into the null operator, allowing us to retrieve the stationary limit $\langle(\Delta h)^4\rangle - \langle(\Delta h)^2\rangle^2$ for the curvature coefficient $\kappa_{\text{AC}}^2(s)$ [13]. The formulation of $\kappa_{\text{AC}}^2(s)$ in Eq. (11) is derived through a method that depends on the computation of expectation values, which necessitate an understanding of the state vector $|\psi(t)\rangle$ governed by the time-dependent Schrödinger's evolution equation. As discussed in Ref. [14], this expectation-values methodology provides a valuable statistical interpretation for $\kappa_{\text{AC}}^2(s)$.

4. Calculation technique: Qubit case

Notwithstanding its statistical significance, $\kappa_{\text{AC}}^2(s)$ in Eq. (11) lacks a definitive geometrical interpretation. This inadequacy prompts an investigation into nonstationary Hamiltonians and two-level quantum systems, leading to the derivation of a closed-form expression for the curvature coefficient associated with a curve delineated by a single-qubit quantum state evolving under an arbitrary nonstationary Hamiltonian. The curvature coefficient κ_{AC}^2 can be articulated entirely in terms of two distinct real three-dimensional vectors that possess a clear geometric meaning. In particular, these vectors are the Bloch vector $\mathbf{a}(t)$ and the magnetic field vector $\mathbf{h}(t)$. While $\mathbf{a}(t)$ arises from the

density operator $\rho(t) = |\psi(t)\rangle\langle\psi(t)| \stackrel{\text{def}}{=} [\mathbf{1} + \mathbf{a}(t) \cdot \boldsymbol{\sigma}] / 2$, $\mathbf{h}(t)$ defines the nonstationary Hamiltonian $H(t) \stackrel{\text{def}}{=} \mathbf{h}(t) \cdot \boldsymbol{\sigma}$. Based on the comprehensive examination in Ref. [14], one obtains

$$\kappa_{\text{AC}}^2(\mathbf{a}, \mathbf{h}) = 4 \frac{(\mathbf{a} \cdot \mathbf{h})^2}{\mathbf{h}^2 - (\mathbf{a} \cdot \mathbf{h})^2} + \left\{ \frac{\left[(\mathbf{h}^2)(\dot{\mathbf{h}}^2) - (\mathbf{h} \cdot \dot{\mathbf{h}})^2 \right] - \left[(\mathbf{a} \cdot \dot{\mathbf{h}}) \mathbf{h} - (\mathbf{a} \cdot \mathbf{h}) \dot{\mathbf{h}} \right]^2}{\left[\mathbf{h}^2 - (\mathbf{a} \cdot \mathbf{h})^2 \right]^3} + 4 \frac{(\mathbf{a} \cdot \mathbf{h}) [\mathbf{a} \cdot (\mathbf{h} \times \dot{\mathbf{h}})]}{\left[\mathbf{h}^2 - (\mathbf{a} \cdot \mathbf{h})^2 \right]^2} \right\}. \quad (12)$$

The representation of κ_{AC}^2 in Eq. (12) is highly beneficial from a computational perspective for qubit systems and simultaneously provides a distinct geometric interpretation of the curvature of quantum evolution, expressed in terms of the Bloch vector $\mathbf{a}(t)$ (normalized, with no units) and the magnetic field vector $\mathbf{h}(t)$ (unnormalized, with $[\mathbf{h}]_{\text{MKS}} = \text{joules} \cdot \text{sec.}^{-1}$ when letting $\hbar = 1$).

Having elucidated the method for calculating the curvature coefficient of quantum evolution in two-level systems, we can now proceed to describe the complexity of quantum evolution on the Bloch sphere.

B. Complexity

In continuation of the research outlined in Refs. [34, 35], we assess the single-qubit quantum dynamics governed by both stationary and nonstationary Hamiltonian evolutions over a defined time interval $[t_A, t_B]$ by defining the complexity $C(t_A, t_B)$ as

$$C(t_A, t_B) \stackrel{\text{def}}{=} \frac{V_{\text{max}}(t_A, t_B) - \bar{V}(t_A, t_B)}{V_{\text{max}}(t_A, t_B)}. \quad (13)$$

The rationale behind proposing this expression for the complexity $C(t_A, t_B)$ will be elucidated in the subsequent paragraphs.

We commence by defining $\bar{V}(t_A, t_B)$ and $V_{\text{max}}(t_A, t_B)$ as stated in Eq. (13). To articulate the definition of the so-called *accessed volume* $\bar{V}(t_A, t_B)$, we will adopt a schematic approach as follows. If feasible, analytically integrate the time-dependent Schrödinger evolution equation $i\hbar\partial_t |\psi(t)\rangle = H(t)|\psi(t)\rangle$ and represent the (normalized) single-qubit state vector $|\psi(t)\rangle$ at any arbitrary time t in terms of the computational basis state vectors $\{|0\rangle, |1\rangle\}$. If this is not feasible, proceed with a numerical analysis. We derive $|\psi(t)\rangle = c_0(t)|0\rangle + c_1(t)|1\rangle$, with $c_0(t)$ and $c_1(t)$ being recast as

$$c_0(t) \stackrel{\text{def}}{=} \langle 0 | \psi(t) \rangle = |c_0(t)| e^{i\phi_0(t)}, \text{ and } c_1(t) \stackrel{\text{def}}{=} \langle 1 | \psi(t) \rangle = |c_1(t)| e^{i\phi_1(t)}, \quad (14)$$

respectively. Furthermore, it is important to note that $\phi_0(t)$ and $\phi_1(t)$ denote the real phases of $c_0(t)$ and $c_1(t)$, respectively. Subsequently, by utilizing the complex quantum amplitudes $c_0(t)$ and $c_1(t)$ as presented in Eq. (14), reformulate the state $|\psi(t)\rangle$ into a physically equivalent state expressed in its standard Bloch sphere representation, which is defined by the polar angle $\theta(t) \in [0, \pi]$ and the azimuthal angle $\varphi(t) \in [0, 2\pi)$. With the availability of the temporal variations of the two spherical angles $\theta(t)$ and $\varphi(t)$, determine the volume of the parametric region that the quantum-mechanical system explores during its evolution from $|\psi(t_A)\rangle = |A\rangle$ to $|\psi(t)\rangle$. Finally, compute the temporal-average volume of the parametric region traversed by the quantum-mechanical system as it evolves from $|\psi(t_A)\rangle = |A\rangle$ to $|\psi(t_B)\rangle = |B\rangle$ with $t \in [t_A, t_B]$.

In accordance with this preliminary outline, we shall now explore the details of the calculation process for $\bar{V}(t_A, t_B)$. Utilizing Eq. (14), we observe that $|\psi(t)\rangle = c_0(t)|0\rangle + c_1(t)|1\rangle$ is physically equivalent to the state $|c_0(t)| |0\rangle + |c_1(t)| e^{i[\phi_1(t) - \phi_0(t)]} |1\rangle$. Consequently, $|\psi(t)\rangle$ can be reformulated as

$$|\psi(t)\rangle = \cos \left[\frac{\theta(t)}{2} \right] |0\rangle + e^{i\varphi(t)} \sin \left[\frac{\theta(t)}{2} \right] |1\rangle. \quad (15)$$

From a formal perspective, the polar angle $\theta(t)$ and the azimuthal angle $\varphi(t) \stackrel{\text{def}}{=} \phi_1(t) - \phi_0(t) = \arg[c_1(t)] - \arg[c_0(t)]$ in Eq. (15) can be expressed as

$$\theta(t) \stackrel{\text{def}}{=} 2 \arctan \left(\frac{|c_1(t)|}{|c_0(t)|} \right), \quad (16)$$

and, under the conditions that $\text{Re}[c_1(t)] > 0$ and $\text{Re}[c_0(t)] > 0$,

$$\varphi(t) \stackrel{\text{def}}{=} \arctan \left\{ \frac{\text{Im}[c_1(t)]}{\text{Re}[c_1(t)]} \right\} - \arctan \left\{ \frac{\text{Im}[c_0(t)]}{\text{Re}[c_0(t)]} \right\}, \quad (17)$$

respectively.

In general, the functional form for $\varphi(t)$ as presented in Eq. (17) can take on a more convoluted expression. This complication arises from the necessity to express the phase $\arg(z)$ of a complex number $\mathbb{C} \ni z \stackrel{\text{def}}{=} x + iy = |z| e^{i\arg(z)}$ in terms of the 2-argument arctangent function atan2 as $\arg(z) = \text{atan2}(y, x)$. When $x > 0$, the function $\text{atan2}(y, x)$ simplifies to $\arctan(y/x)$. For further mathematical insights regarding atan2 , we recommend consulting Ref. [43]. Therefore, with $\theta(t)$ and $\varphi(t)$ defined, it can be observed that the unit three-dimensional Bloch vector $\mathbf{a}(t)$, which corresponds to the state vector $|\psi(t)\rangle$ as indicated in Eq. (15), is expressed as $\mathbf{a}(t) = (\sin[\theta(t)]\cos[\varphi(t)], \sin[\theta(t)]\sin[\varphi(t)], \cos[\theta(t)])$. At present, we can define $\bar{V}(t_A, t_B)$. In particular, the accessed volume $\bar{V}(t_A, t_B)$, which relates to the quantum evolution directed by the Hamiltonian $H(t)$ from $|\psi(t_A)\rangle = |A\rangle$ to $|\psi(t_B)\rangle = |B\rangle$, where t is within the interval $[t_A, t_B]$, is expressed as

$$\bar{V}(t_A, t_B) \stackrel{\text{def}}{=} \frac{1}{t_B - t_A} \int_{t_A}^{t_B} V(t) dt. \quad (18)$$

From Eq. (18), $\bar{V}(t_A, t_B)$ can be regarded as a mean value of $V(t)$ over the time interval $[t_A, t_B]$. The variable $V(t)$ referenced in Eq. (18) represents the instantaneous volume, which is defined as

$$V(t) = V(\theta(t), \varphi(t)) \stackrel{\text{def}}{=} \text{vol}[\mathcal{D}_{\text{accessed}}[\theta(t), \varphi(t)]], \quad (19)$$

with $\text{vol}[\mathcal{D}_{\text{accessed}}[\theta(t), \varphi(t)]]$ being defined as

$$\text{vol}[\mathcal{D}_{\text{accessed}}[\theta(t), \varphi(t)]] \stackrel{\text{def}}{=} \int \int_{\mathcal{D}_{\text{accessed}}[\theta(t), \varphi(t)]} \sqrt{g_{\text{FS}}(\theta, \varphi)} d\theta d\varphi. \quad (20)$$

We note that $\text{vol}[\cdot]$ stands for $|\text{vol}[\cdot]| \geq 0$, given our consideration of these volumes as defined by positive real numerical values. In Eq. (20), $g_{\text{FS}}(\theta, \varphi) \stackrel{\text{def}}{=} \sqrt{\sin^2(\theta)/16}$ represents the determinant of the matrix linked to the Fubini-Study infinitesimal line element $ds_{\text{FS}}^2 \stackrel{\text{def}}{=} (1/4) [d\theta^2 + \sin^2(\theta)d\varphi^2]$. Finally, $\mathcal{D}_{\text{accessed}}[\theta(t), \varphi(t)]$ in Eq. (20) specifies the parametric region that the quantum-mechanical system explores during its transition from the initial state $|\psi(t_A)\rangle = |A\rangle$ to an intermediate state $|\psi(t)\rangle$, where $t \in [t_A, t_B]$. It is expressed as

$$\mathcal{D}_{\text{accessed}}[\theta(t), \varphi(t)] \stackrel{\text{def}}{=} [\theta(t_A), \theta(t)] \times [\varphi(t_A), \varphi(t)] \subset [0, \pi]_\theta \times [0, 2\pi]_\varphi. \quad (21)$$

To enhance computational efficiency, we observe that the instantaneous volume $V(t)$ in Eq. (19) can be easily reformulated as $V(t) = |(\cos[\theta(t_A)] - \cos[\theta(t)]) (\varphi(t) - \varphi(t_A))|/4$, where $\theta(t)$ and $\varphi(t)$ are defined Eqs. (16) and (17), respectively. In conclusion, assuming that the tilde symbol denotes the time-average process, the accessed volume $\bar{V}(t_A, t_B)$ in Eq. (18) can be expressed as

$$\bar{V}(t_A, t_B) \stackrel{\text{def}}{=} \tilde{\text{vol}}[\mathcal{D}_{\text{accessed}}[\theta(t), \varphi(t)]], \quad (22)$$

with $t \in [t_A, t_B]$ in Eq. (22). Finally, in accordance with the physical motivations presented in Refs. [34, 35], the accessible volume $V_{\text{max}}(t_A, t_B)$ in Eq. (13) is defined as

$$V_{\text{max}}(t_A, t_B) \stackrel{\text{def}}{=} \text{vol}[\mathcal{D}_{\text{accessible}}(\theta, \varphi)] = \int \int_{\mathcal{D}_{\text{accessible}}(\theta, \varphi)} \sqrt{g_{\text{FS}}(\theta, \varphi)} d\theta d\varphi. \quad (23)$$

The quantity $\mathcal{D}_{\text{accessible}}(\theta, \varphi)$ mentioned in Eq. (23) denotes the (local) maximally accessible two-dimensional parametric region that occurs during the quantum-mechanical transition from $|\psi_A(\theta_A, \varphi_A)\rangle$ to $|\psi(\theta_B, \varphi_B)\rangle$ and is defined by

$$\mathcal{D}_{\text{accessible}}(\theta, \varphi) \stackrel{\text{def}}{=} \{(\theta, \varphi) : \theta_{\min} \leq \theta \leq \theta_{\max}, \text{ and } \varphi_{\min} \leq \varphi \leq \varphi_{\max}\}. \quad (24)$$

It is important to note that θ_{\min} , θ_{\max} , φ_{\min} , and φ_{\max} as presented in Eq. (24) are defined as

$$\theta_{\min} \stackrel{\text{def}}{=} \min_{t_A \leq t \leq t_B} \theta(t), \theta_{\max} \stackrel{\text{def}}{=} \max_{t_A \leq t \leq t_B} \theta(t), \varphi_{\min} \stackrel{\text{def}}{=} \min_{t_A \leq t \leq t_B} \varphi(t), \text{ and } \varphi_{\max} \stackrel{\text{def}}{=} \max_{t_A \leq t \leq t_B} \varphi(t), \quad (25)$$

in that order. Additionally, it should be observed that $\mathcal{D}_{\text{accessed}}(\theta, \varphi) \subset \mathcal{D}_{\text{accessible}}(\theta, \varphi) \subset [0, \pi]_\theta \times [0, 2\pi]_\varphi$. Lastly, with $\bar{V}(t_A, t_B)$ and $V_{\text{max}}(t_A, t_B)$ available in Eqs. (18) and (23), respectively, we can formally define our proposed complexity notion $C(t_A, t_B)$ in Eq. (13).

In general terms, we assess the complexity of a quantum evolution from an initial state to a final state on the Bloch sphere by considering the proportion of the non-accessed volume of the sphere that lies within the accessible volume of the sphere itself. Specifically, when the accessible volume is predominantly (minimally) explored, the complexity is low (high). For more details, we refer to Refs. [34, 35].

Before transitioning to the next section, we highlight that in the dynamics of qubits, the curvature coefficient κ_{AC}^2 in Eq. (12) is solely dependent on the Bloch vector \mathbf{a} and the magnetic field vector \mathbf{h} . To experimentally determine \mathbf{a} , one can conduct quantum measurements of the expectation values of the Pauli spin operators $\langle \sigma_x \rangle$, $\langle \sigma_y \rangle$, and $\langle \sigma_z \rangle$ because $\mathbf{a}(t) = \text{tr}[\rho(t)\sigma]$ with $\rho(t) = [\mathbf{1} + \mathbf{a}(t) \cdot \boldsymbol{\sigma}] / 2$. Furthermore, from the Bloch equation $\dot{\mathbf{a}} = 2\mathbf{h} \times \mathbf{a}$, it is evident that only the component of \mathbf{h} that is orthogonal to \mathbf{a} influences the trajectory of \mathbf{a} . Consequently, by utilizing \mathbf{a} and its derivative $\dot{\mathbf{a}}$, one can reconstruct the plane of rotation, thereby determining the axis of rotation \mathbf{h} , up to a global energy shift that does not alter the state on the Bloch sphere. Regarding our complexity measure C in Eq. (13) for qubit dynamics, it can essentially be derived from the spherical angles representing a qubit state on the Bloch sphere. Considering the fact that

$$\mathbf{a}(t) = (\sin(\theta_t) \cos(\varphi_t), \sin(\theta_t) \sin(\varphi_t), \cos(\theta_t)) = (\langle \sigma_x \rangle(t), \langle \sigma_y \rangle(t), \langle \sigma_z \rangle(t)), \quad (26)$$

one can experimentally determine the polar and azimuthal angles $\theta_t = \theta(t)$ and $\varphi_t = \varphi(t)$ from the measurements of the expectation values of the Pauli operators. In particular, we have

$$\theta(t) = \arccos[\langle \sigma_z \rangle(t)], \text{ and } \varphi(t) = \text{atan2}(\langle \sigma_y \rangle(t), \langle \sigma_x \rangle(t)), \quad (27)$$

where $\text{atan2}(\cdot, \cdot)$ is the previously mentioned 2-argument arctangent function with $\text{atan2}(\langle \sigma_y \rangle(t), \langle \sigma_x \rangle(t)) = \arctan[\langle \sigma_y \rangle(t) / \langle \sigma_x \rangle(t)]$ if $\langle \sigma_x \rangle(t) > 0$.

With these final observations, we are now prepared to present the Hamiltonian model that we intend to investigate.

IV. HAMILTONIAN MODEL

In this section, we present a two-parameter family of time-varying Hamiltonians, which we intend to analyze from a geometric perspective. Specifically, we focus on the time-dependent configurations of the magnetic fields that characterize the Hamiltonians, along with the temporal dynamics of the phase that dictates the relative phase factor involved in the decomposition of the evolving state in relation to the computational basis state vectors.

A. Preliminaries

In Ref. [36], the most thorough Hermitian nonstationary qubit Hamiltonian $H(t)$ is constructed in such a manner that it generates the same motion $\pi(|\psi(t)\rangle)$ within the complex projective Hilbert space $\mathbb{C}P^1$ (or, equivalently, on the Bloch sphere $S^2 \cong \mathbb{C}P^1$) as $|\psi(t)\rangle$, where the projection operator π is such that $\pi : \mathcal{H}_2^1 \ni |\psi(t)\rangle \mapsto \pi(|\psi(t)\rangle) \in \mathbb{C}P^1$. In general, it can be shown that $H(t)$ is expressible as

$$H(t) = iE|\partial_t m(t)\rangle\langle m(t)| - iE|m(t)\rangle\langle\partial_t m(t)|, \quad (28)$$

where, for simplicity, we define $|m(t)\rangle = |m\rangle$, $|\partial_t m(t)\rangle = |\dot{m}\rangle$, $E = 1$ and, lastly, $\hbar = 1$. The unit state vector $|m\rangle$ fulfills the relations $\pi(|m(t)\rangle) = \pi(|\psi(t)\rangle)$ and $i\partial_t|m(t)\rangle = H(t)|m(t)\rangle$. The condition $\pi(|m(t)\rangle) = \pi(|\psi(t)\rangle)$ results in the conclusion that $|m(t)\rangle = c(t)|\psi(t)\rangle$, where $c(t)$ represents a complex function. By asserting that $\langle m|m \rangle = 1$, we deduce that $|c(t)| = 1$. This condition implies, consequently, that $c(t) = e^{i\phi(t)}$ for a specific real phase $\phi(t)$. Next, by utilizing the parallel transport condition $\langle m|\dot{m} \rangle = \langle \dot{m}|m \rangle = 0$, the phase $\phi(t)$ is established as $i \int \langle \psi | \dot{\psi} \rangle dt$. As a consequence, $|m(t)\rangle = \exp(-\int_0^t \langle \psi(t') | \partial_{t'} \psi(t') \rangle dt')|\psi(t)\rangle$. It is crucial to highlight that $H(t)$ in Eq. (28) is fundamentally traceless, as it comprises solely off-diagonal elements with respect to the orthogonal basis $\{|m\rangle, |\partial_t m\rangle\}$. Also, $H(t)$ is a linear combination of traceless Pauli spin matrices. Lastly, the condition $i\partial_t|m(t)\rangle = H(t)|m(t)\rangle$ signifies that $|m(t)\rangle$ complies with the Schrödinger evolution equation.

After presenting some essential preliminary information regarding Uzdin's research in Ref. [36], we are now prepared to introduce our proposed time-dependent Hamiltonian.

B. The Hamiltonian

To begin, let us consider the normalized state vector $|\psi(t)\rangle$ defined as,

$$|\psi(t)\rangle \stackrel{\text{def}}{=} \cos[\alpha(t)]|0\rangle + e^{i\beta(t)}\sin[\alpha(t)]|1\rangle, \quad (29)$$

with $\alpha(t)$ and $\beta(t)$ being two generally time-dependent real parameters. From Eq. (29), we note that $\langle \psi(t) | \dot{\psi}(t) \rangle = i\dot{\beta}(t) \sin^2[\alpha(t)] \neq 0$. Therefore, let us find $|m(t)\rangle = e^{-i\phi(t)} |\psi(t)\rangle$, with $\langle m(t) | \dot{m}(t) \rangle = 0$. We observe that $\langle m(t) | \dot{m}(t) \rangle = 0$ if and only if $\dot{\phi}(t) = -i \langle \psi(t) | \dot{\psi}(t) \rangle = \dot{\beta}(t) \sin^2([\alpha(t)])$, that is

$$\phi(t) = \int_0^t \dot{\beta}(t') \sin^2[\alpha(t')] dt'. \quad (30)$$

Given $|\psi(t)\rangle$ and $\phi(t)$ in Eqs. (29) and (30), respectively, the state $|m(t)\rangle$ reduces to

$$|m(t)\rangle = e^{-i \int_0^t \dot{\beta}(t') \sin^2[\alpha(t')] dt'} \left\{ \cos[\alpha(t)] |0\rangle + e^{i\beta(t)} \sin[\alpha(t)] |1\rangle \right\}, \quad (31)$$

Setting $|m\rangle \langle m| = (1/2) (\mathbf{1} + \mathbf{a} \cdot \boldsymbol{\sigma})$, use of Eq. (31) leads to the expression of the Bloch vector $\mathbf{a}(t)$ in terms of the real time-dependent parameters $\alpha(t)$ and $\beta(t)$,

$$\mathbf{a} \stackrel{\text{def}}{=} \begin{pmatrix} a_x \\ a_y \\ a_z \end{pmatrix} = \begin{pmatrix} \sin(2\alpha) \cos(\beta) \\ \sin(2\alpha) \sin(\beta) \\ \cos(2\alpha) \end{pmatrix}. \quad (32)$$

From Eq. (32), we note that $\mathbf{a} \cdot \mathbf{a} = a_x^2 + a_y^2 + a_z^2 = 1$. Lastly, to find the the expression of $\mathbf{H}(t) = i |\partial_t m(t)\rangle \langle m(t)| - i |m(t)\rangle \langle \partial_t m(t)|$ recast as $h_0(t) \mathbf{1} + \mathbf{h}(t) \cdot \boldsymbol{\sigma}$, we need to find the explicit formulae for both $h_0(t)$ and the magnetic field vector $\mathbf{h}(t)$. After some algebraic manipulations, we arrive at

$$\begin{aligned} \mathbf{H}(t) &= \begin{pmatrix} h_0 + h_z & h_x - ih_y \\ h_x + ih_y & h_0 - h_z \end{pmatrix} \\ &= \begin{pmatrix} 2\dot{\phi} \cos^2(\alpha) & e^{-i\beta} [2\dot{\phi} \sin(\alpha) \cos(\alpha) - i\dot{\alpha} - \dot{\beta} \sin(\alpha) \cos(\alpha)] \\ e^{i\beta} [2\dot{\phi} \sin(\alpha) \cos(\alpha) + i\dot{\alpha} - \dot{\beta} \sin(\alpha) \cos(\alpha)] & 2\dot{\phi} \sin^2(\alpha) - 2\dot{\beta} \sin^2(\alpha) \end{pmatrix}. \end{aligned} \quad (33)$$

From Eq. (33), we determine that $h_0(t) = 0$ (as expected, since the Hamiltonian is traceless). In addition, using Eq. (30), we note from Eq. (33) that $\mathbf{h}(t)$ equals

$$\mathbf{h}(t) \stackrel{\text{def}}{=} \begin{pmatrix} h_x(t) \\ h_y(t) \\ h_z(t) \end{pmatrix} = \begin{pmatrix} -\frac{\dot{\beta}}{2} \cos(2\alpha) \sin(2\alpha) \cos(\beta) - \dot{\alpha} \sin(\beta) \\ -\frac{\dot{\beta}}{2} \cos(2\alpha) \sin(2\alpha) \sin(\beta) + \dot{\alpha} \cos(\beta) \\ \frac{\dot{\beta}}{2} \sin^2(2\alpha) \end{pmatrix}. \quad (34)$$

By employing Eqs. (32) and (34), one can verify through some simple but laborious algebra that the Bloch vector and the magnetic vector fulfill the differential equation $\dot{\mathbf{a}} = 2\mathbf{h} \times \mathbf{a}$ [1]. For completeness, we remark that up to constant factors, this vector differential equation characterizes the Larmor precession described by the equation $d\mathbf{m}/dt = \gamma \mathbf{m} \times \mathbf{B}$, with \mathbf{m} being the magnetic moment vector, \mathbf{B} denoting the external magnetic moment, and γ representing the gyromagnetic ratio. Interestingly, we note that the Bloch vector $\mathbf{a}(t)$ in Eq. (32) and the magnetic field $\mathbf{h}(t)$ in Eq. (34) are orthogonal since $\mathbf{a} \cdot \mathbf{h} = 0$ at any time. Observe that $\dot{\mathbf{a}} = 2\mathbf{h} \times \mathbf{a}$ implies that $\dot{\mathbf{a}} \cdot \mathbf{h} = 0$. Therefore, since $\mathbf{a} \cdot \mathbf{h} = 0$ implies that $\dot{\mathbf{a}} \cdot \mathbf{h} + \mathbf{a} \cdot \dot{\mathbf{h}} = 0$, we also have $\mathbf{a} \cdot \dot{\mathbf{h}} = 0$. In summary, we have the following relations: (i) $\dot{\mathbf{a}} = 2\mathbf{h} \times \mathbf{a}$, which implies $\dot{\mathbf{a}} \cdot \mathbf{h} = 0$; (ii) $\mathbf{a} \cdot \mathbf{h} = 0$, which implies $\dot{\mathbf{a}} \cdot \mathbf{h} + \mathbf{a} \cdot \dot{\mathbf{h}} = 0$; (iii) $\mathbf{a} \cdot \dot{\mathbf{h}} = 0$, as a consequence of (i) and (ii). Exploiting these geometric constraints between the Bloch and magnetic vectors, the curvature coefficient $\kappa_{AC}^2(\mathbf{a}, \mathbf{h})$ in Eq. (12) reduces to

$$\kappa_{AC}^2(\mathbf{h}) = \frac{(\mathbf{h}^2)(\dot{\mathbf{h}}^2) - (\mathbf{h} \cdot \dot{\mathbf{h}})^2}{\mathbf{h}^6}. \quad (35)$$

Lastly, we note that $\|\mathbf{h}\|^2 = (\dot{\beta}^2/4) \sin^2(2\alpha) + \dot{\alpha}^2$, we realize that the magnetic field vector $\mathbf{h}(t)$ in Eq. (34) can be recast as $\mathbf{h}(t) = \mathcal{R}_{\hat{z}}[\beta(t)] \mathbf{h}_0(t)$. More specifically, assuming $(\dot{\beta}/2) \sin(2\alpha) \geq 0$, we can describe $\mathbf{h}(t)$ in a matrix form as

$$\begin{pmatrix} h_x \\ h_y \\ h_z \end{pmatrix} = \mathcal{R}_{\hat{z}}[\beta(t)] \begin{pmatrix} -\sqrt{\|\mathbf{h}\|^2 - \dot{\alpha}^2} \cos(2\alpha) \\ \dot{\alpha} \\ +\sqrt{\|\mathbf{h}\|^2 - \dot{\alpha}^2} \cos(2\alpha) \end{pmatrix}. \quad (36)$$

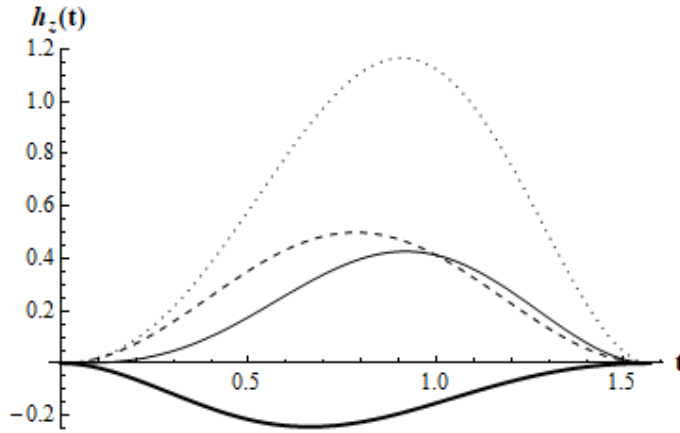


FIG. 1: Temporal behavior of the magnetic field vector projected onto the \hat{z} -axis when the phase $\beta(t)$ exhibits exponential decay (thick solid line), quadratic growth (thin solid line), linear growth (dashed line) and, finally, exponential growth (dotted line). In all plots, we set $\nu_0 = \omega_0 = 1$ and $0 \leq t \leq \pi/2$. Physical units are chosen using $\hbar = 1$.

When $(\dot{\beta}/2) \sin(2\alpha) \leq 0$, the signs of the first and third components of $\mathbf{h}_0(t)$ in the right-hand-side of Eq. (36) are reversed. Therefore, Eq. (36) implies that $\mathbf{h}(t)$ can be described in terms of a rotation $\mathcal{R}_{\hat{z}}[\beta(t)]$ about the \hat{z} -axis by a varying angle $\beta(t)$ of a nonstationary magnetic vector $\mathbf{h}_0(t)$. In particular, when $\beta(t)$ remains constant in time with $\beta(t) = \beta_0$, we have $\|\mathbf{h}\|^2 = \dot{\alpha}^2$, $\mathbf{h}_0 = (0, \dot{\alpha}, 0)$, and $\mathbf{h} = (-\dot{\alpha} \sin(\beta_0), \dot{\alpha} \cos(\beta_0), 0)$. In Fig. 1, we illustrate the temporal behavior of the magnetic field vector projected onto the z -axis in the various scenarios specified by $\beta(t)$ that will be discussed subsequently.

We are now ready for our applications.

V. APPLICATIONS

In this section, we employ the concepts presented in Sections II and III to characterize the quantum evolutions outlined in Section IV. Specifically, by concentrating on the temporal dependence of the previously mentioned phase $\beta(t)$, we analyze five different scenarios: i) no growth; ii) linear growth; iii) quadratic growth; iv) exponential growth; v) exponential decay.

More specifically, we present a comparative analysis of various quantum evolutions, focusing on the concepts of efficiency, curvature, and complexity that were introduced earlier. These evolutions are defined by unique magnetic field configurations $\mathbf{h}(t)$, which are influenced by the generally time-dependent real parameters $\alpha(t)$ and $\beta(t)$. Specifically, $\alpha(t)$ dictates the temporal behavior of the quantum amplitudes of the evolving state $|\psi(t)\rangle$ in relation to the computational basis vectors $|0\rangle$ and $|1\rangle$, while $\beta(t)$ describes the quantum-mechanically observable relative phase factor that is included in the expression of $|\psi(t)\rangle$. We particularly concentrate on quantum evolutions that transition between orthogonal initial and final states $|A\rangle \stackrel{\text{def}}{=} |\psi(0)\rangle = |0\rangle$ and $|B\rangle \stackrel{\text{def}}{=} |\psi(t_{\text{final}})\rangle \simeq |1\rangle$. Furthermore, to highlight the changes in motion caused by different time-configurations of the relative phase factor defined by $\beta(t)$, we will set $\alpha(t) \stackrel{\text{def}}{=} \omega_0 t$ with $\omega_0 \in \mathbb{R}_+ \setminus \{0\}$, for the entirety of our comparative analysis. Based on the expression of $|\psi(t)\rangle$, the aforementioned assumption regarding $\alpha(t)$ leads us to take t_{final} as equal to $\pi/(2\omega_0)$. For a schematic overview of selected geometric features of nonstationary Hamiltonian evolutions on the Bloch sphere, we suggest looking at Table I.

A. No growth

In the first example, we assume that $\mathbf{h}(t)$ is characterized by a phase $\beta(t)$ that does not change in time. In particular, we set $\beta(t) \stackrel{\text{def}}{=} \beta_0 \in \mathbb{R}_+ \setminus \{0\}$ so that $\dot{\beta} = 0$. The evolution of interest occurs from $|A\rangle = |0\rangle$ to $|B\rangle \simeq |1\rangle$ in a temporal interval $t_{\text{final}} = \pi/(2\omega_0)$, recalling our choice with $\alpha(t)$ being equal to $\omega_0 t$. The symbol “ \simeq ” denotes physical equivalence of quantum states, modulo unimportant global phase factors.

Type of phase, $\beta(t)$	Geodesic efficiency, η_{GE}	Speed efficiency, η_{SE}	Curvature, κ_{AC}^2	Complexity, C
No growth	1	1	0	Constant
Linear growth	< 1	1	> 0	Constant
Quadratic growth	< 1	1	> 0	Constant
Exponential growth	< 1	1	> 0	Non-constant
Exponential decay	< 1	1	> 0	Non-constant

TABLE I: Schematic overview of selected geometric features of nonstationary Hamiltonian evolutions on the Bloch sphere. In particular, for each evolution defined by a specific time-dependent phase that determines the local phase factor of the evolving state vector, we examined the geodesic efficiency η_{GE} , speed efficiency η_{SE} , curvature coefficient κ_{AC}^2 , and ultimately, the complexity C of the dynamical trajectory on the Bloch sphere that is determined by the aforementioned state vector. Note that, in general, $\eta_{\text{GE}} = \eta_{\text{GE}}(\omega_0, \nu_0)$, $\eta_{\text{SE}} = \eta_{\text{SE}}(t; \omega_0, \nu_0)$, $\kappa_{\text{AC}}^2 = \kappa_{\text{AC}}^2(t; \omega_0, \nu_0)$, and $C = C(\omega_0, \nu_0)$. For instance, focusing on global (i.e., non instantaneous) quantities such as the geodesic efficiency η_{GE} and the complexity C and, in addition, setting $\omega_0 = \nu_0 = 1$, we have: $\eta_{\text{GE}}^{(\text{No growth})} = 1$, $\eta_{\text{GE}}^{(\text{Linear growth})} \simeq 0.94$, $\eta_{\text{GE}}^{(\text{Quadratic growth})} \simeq 0.96$, $\eta_{\text{GE}}^{(\text{Exponential growth})} \simeq 0.78$, $\eta_{\text{GE}}^{(\text{Exponential decay})} \simeq 0.98$, $C^{(\text{No growth})} = 0.5$, $C^{(\text{Linear growth})} \simeq 0.65$, $C^{(\text{Quadratic growth})} \simeq 0.73$, $C^{(\text{Exponential growth})} \simeq 0.71$, and $C^{(\text{Exponential decay})} \simeq 0.59$. For more details, we refer to the main sections of this manuscript.

Geodesic efficiency. From a geodesic efficiency standpoint, we note that the geodesic distance s_0 from $|A\rangle$ to $|B\rangle$ is $s_0 = \pi$. Moreover, the energy uncertainty $\Delta E(t) = \sqrt{\langle \dot{m} | \dot{m} \rangle}$ is constant and equals ω_0 since $\langle \dot{m} | \dot{m} \rangle = \dot{\alpha}^2 + (1/4)\dot{\beta}^2 \sin^2(2\alpha)$. Therefore, this evolution happens with unit geodesic efficiency, $\eta_{\text{GE}} = 1$, since $s = s_0 = \pi$. We stress that the magnetic field vector $\mathbf{h}(t)$ has no longitudinal vector component (i.e., $\mathbf{h}_{\parallel}(t) = \mathbf{0}$) since the Bloch vector $\mathbf{a}(t)$ and $\mathbf{h}(t)$ are orthogonal for any $0 \leq t \leq \pi/(2\omega_0)$. Indeed, $\mathbf{h}(t)$ is completely transverse since $\mathbf{h}(t) = \mathbf{h}_{\perp}(t)$ and, in addition, $h_{\perp}(t) = \sqrt{\mathbf{h}_{\perp} \cdot \mathbf{h}_{\perp}} = \omega_0$ is constant in time.

Speed efficiency. From a speed efficiency standpoint, the evolution occurs with $\eta_{\text{SE}}(t) = 1$ for any $0 \leq t \leq \pi/(2\omega_0)$. This is justified by construction, given the choice of the Hamiltonian $H(t)$. In addition, the unit speed efficiency can also be understood by noticing that magnetic field vector $\mathbf{h}(t)$, as previously mentioned, has no longitudinal vector component (i.e., $\mathbf{h}_{\parallel}(t) = \mathbf{0}$). It is indeed the longitudinal vector component of a magnetic field the one that has a detrimental effect on the motion since its presence limits the fraction of energy of the systems used for its quantum evolution with a high speed (i.e., $\Delta E(t) \leq \|H(t)\|_{\text{SP}}$ when $\mathbf{h}_{\parallel}(t) \neq \mathbf{0}$).

Curvature. The curvature coefficient κ_{AC}^2 of this quantum evolution is zero. This is in agreement with the fact that $\eta_{\text{GE}} = 1$. From a magnetic field perspective, we have $\mathbf{h}^2 = \dot{\alpha}^2$, $\dot{\mathbf{h}}^2 = \ddot{\alpha}^2$, and $(\mathbf{h} \cdot \dot{\mathbf{h}})^2 = \dot{\alpha}^2 \ddot{\alpha}^2$. Therefore, the vanishing of the curvature coefficient is a consequence of the fact that $\mathbf{h}(t)$ and $\dot{\mathbf{h}}(t)$ are collinear (i.e., $\partial_t \hat{h}(t) = \mathbf{0}$, with $\mathbf{h}(t) = h(t)\hat{h}(t)$). In other words, the magnetic field changes only in intensity, but not in direction.

Complexity. Finally, from a complexity viewpoint, we have that $\theta(t) = 2\omega_0 t$ and $\varphi(t) = \beta_0$, with $0 \leq \theta \leq \pi$ and $0 \leq t \leq \pi/(2\omega_0)$. Therefore, a straightforward calculation yields expressions for instantaneous, accessed, and accessible volumes $V(t) = \omega_0 t$, $\bar{V} = \pi/4$, and $V_{\text{max}} = \pi/2$, respectively. Therefore, the complexity of this quantum evolution reduces to $C = 1/2$.

B. Linear growth

In the second example, we suppose that $\mathbf{h}(t)$ is characterized by a phase $\beta(t)$ that grows linearly in time. More specifically, we put $\beta(t) \stackrel{\text{def}}{=} \nu_0 t$ with $\nu_0 \in \mathbb{R}_+ \setminus \{0\}$ so that $\dot{\beta} = \nu_0$. The evolution of focus happens from $|A\rangle = |0\rangle$ to $|B\rangle \simeq |1\rangle$ in a time interval $t_{\text{final}} = \pi/(2\omega_0)$ once one recalls our choice specified by $\alpha(t) = \omega_0 t$.

Geodesic efficiency. From a geodesic efficiency perspective, we observe that the geodesic distance s_0 from $|A\rangle$ to $|B\rangle$ equals $s_0 = \pi$. Moreover, the energy uncertainty $\Delta E(t) = \sqrt{\langle \dot{m} | \dot{m} \rangle}$ is not constant since $\langle \dot{m} | \dot{m} \rangle = \dot{\alpha}^2 + (1/4)\dot{\beta}^2 \sin^2(2\alpha)$ yields $\Delta E^2(t) = \omega_0^2 + (1/4)\nu_0^2 \sin^2(2\omega_0 t)$. Therefore, this evolution occurs with a non unit geodesic efficiency, $\eta_{\text{GE}} < 1$, since $s > s_0 = \pi$. In general, the quantity η_{GE} is a function of the parameters ω_0 and ν_0 and, in particular, can be numerically estimated. For instance, for $\omega_0 = \nu_0 = 1$, $s \simeq 3.33 \geq \pi = s_0$. Similarly to the previous example, the magnetic field vector $\mathbf{h}(t)$ has no longitudinal vector component and, moreover, is completely transverse since $\mathbf{h}(t) = \mathbf{h}_{\perp}(t)$. Unlike the previous case, however, $h_{\perp}(t) = \sqrt{\mathbf{h}_{\perp} \cdot \mathbf{h}_{\perp}}$ is not constant in time since $h_{\perp}(t) = \sqrt{\omega_0^2 + (1/4)\nu_0^2 \sin^2(2\omega_0 t)}$.

Speed efficiency. From a speed efficiency viewpoint, the evolution happens with $\eta_{\text{SE}}(t) = 1$ for any $0 \leq t \leq \pi/(2\omega_0)$. Like in the first example, this happens thanks to the functional form of the Hamiltonian $H(t)$. In addition, the unit speed efficiency can also be explained in terms of the vanishing longitudinal vector component (i.e., $\mathbf{h}_{\parallel}(t) = \mathbf{0}$) of the magnetic field vector $\mathbf{h}(t)$.

Curvature. The curvature coefficient κ_{AC}^2 of this quantum evolution is not equal to zero. This is in agreement with the fact that $\eta_{\text{GE}} < 1$. After some algebra, κ_{AC}^2 in Eq. (12) reduces to

$$[\kappa_{\text{AC}}^2(t; \omega_0, \nu_0)]_{\text{Example-2}} = \frac{\mathbf{h}^2(t; \omega_0, \nu_0) \dot{\mathbf{h}}^2(t; \omega_0, \nu_0) - [\mathbf{h}(t; \omega_0, \nu_0) \cdot \dot{\mathbf{h}}(t; \omega_0, \nu_0)]^2}{\mathbf{h}^6(t; \omega_0, \nu_0)}, \quad (37)$$

where \mathbf{h}^2 , $\dot{\mathbf{h}}^2$, and $(\mathbf{h} \cdot \dot{\mathbf{h}})^2$ in Eq. (37) are given by

$$\begin{aligned} \mathbf{h}^2 &\stackrel{\text{def}}{=} \frac{1}{8}\nu_0^2 + \omega_0^2 - \frac{1}{8}\nu_0^2 \cos(4\omega_0 t), \\ \dot{\mathbf{h}}^2 &\stackrel{\text{def}}{=} \frac{1}{32}\nu_0^4 - \frac{1}{32}\nu_0^4 \cos(8\omega_0 t) + 2\nu_0^2\omega_0^2 + 2\nu_0^2\omega_0^2 \cos(4\omega_0 t), \\ \mathbf{h} \cdot \dot{\mathbf{h}} &\stackrel{\text{def}}{=} \frac{1}{4}\nu_0^2\omega_0 \sin(4\omega_0 t), \end{aligned} \quad (38)$$

respectively. As a side note, we observe that the short-time limit of $[\kappa_{\text{AC}}^2(t; \omega_0, \nu_0)]_{\text{Example-2}}$ is expressed as

$$[\kappa_{\text{AC}}^2(t; \omega_0, \nu_0)]_{\text{Example-2}} \xrightarrow{t \rightarrow 0} 4\left(\frac{\nu_0}{\omega_0}\right)^2 - 8\left(\frac{\nu_0}{\omega_0}\right)^2(\nu_0^2 + 2\omega_0^2)t^2 + \mathcal{O}(t^3), \quad (39)$$

with $[\kappa_{\text{AC}}^2(t; \omega_0, \nu_0)]_{\text{Example-2}}$ commencing at the nonzero value of $4(\nu_0/\omega_0)^2$ at $t = 0$. Lastly, the presence of a non-vanishing curvature coefficient is due to the fact that $\mathbf{h}(t)$ and $\dot{\mathbf{h}}(t)$ are not collinear (i.e., $\partial_t \hat{h}(t) \neq \mathbf{0}$, with $\mathbf{h}(t) = h(t)\hat{h}(t)$). In other terms, unlike what happens in the first example, the magnetic field changes both in intensity and direction.

Complexity. Finally, from a complexity viewpoint, we have that $\theta(t) = 2\omega_0 t$ and $\varphi(t) = \nu_0 t$, with $0 \leq \theta \leq \pi$, $0 \leq \varphi \leq (\pi/2)(\nu_0/\omega_0)$, and $0 \leq t \leq \pi/(2\omega_0)$. Therefore, a straightforward calculation yields expressions for instantaneous, accessed, and accessible volumes

$$V(t) = \frac{\nu_0}{4} [1 - \cos(2\omega_0 t)] t, \quad \bar{V} = \left(\frac{1}{4\pi} + \frac{\pi}{16}\right) \frac{\nu_0}{\omega_0}, \quad \text{and} \quad V_{\text{max}} = \frac{\pi}{4} \frac{\nu_0}{\omega_0}, \quad (40)$$

respectively. Therefore, the complexity of this quantum evolution reduces to

$$C = \frac{3\pi^2 - 4}{4\pi^2}. \quad (41)$$

Interestingly, we note that $[C]_{\text{Example-2}}$ in Eq. (41) is approximately equal to 0.65 and is greater than $[C]_{\text{Example-1}} = 0.5$. It is noteworthy that in the linear growth scenario, the complexity C in Eq. (41) reaches a constant value that is independent of the parameters ω_0 and ν_0 , which arises from the fact that both \bar{V} and V_{max} are proportional to the ratio (ν_0/ω_0) .

C. Quadratic growth

In the third example, we assume that $\mathbf{h}(t)$ is specified by a phase $\beta(t)$ that grows quadratically in time. More precisely, we set $\beta(t) \stackrel{\text{def}}{=} (1/2)\nu_0^2 t^2$ with $\nu_0 \in \mathbb{R}_+ \setminus \{0\}$ so that $\dot{\beta} = \nu_0^2 t$. Recalling that $\alpha(t) = \omega_0 t$, the evolution we study occurs from $|A\rangle = |0\rangle$ to $|B\rangle \simeq |1\rangle$ in a time interval $t_{\text{final}} = \pi/(2\omega_0)$.

Geodesic efficiency. From a geodesic efficiency standpoint, we note that the geodesic distance s_0 from $|A\rangle$ to $|B\rangle$ is equal to $s_0 = \pi$. Furthermore, the energy uncertainty $\Delta E(t) = \sqrt{\langle \dot{m} | \dot{m} \rangle}$ changes in time because $\langle \dot{m} | \dot{m} \rangle = \dot{\alpha}^2 + (1/4)\dot{\beta}^2 \sin^2(2\alpha)$ leads to $\Delta E^2(t) = \omega_0^2 + (1/4)\nu_0^4 t^2 \sin^2(2\omega_0 t)$. Consequently, the quantum evolution in this third scenario happens with a geodesic efficiency $\eta_{\text{GE}} < 1$ because $s > s_0 = \pi$. Similarly to the second scenario, the term η_{GE} depends on the two parameters ω_0 and ν_0 . In this case there is no simple closed form (i.e., analytical)

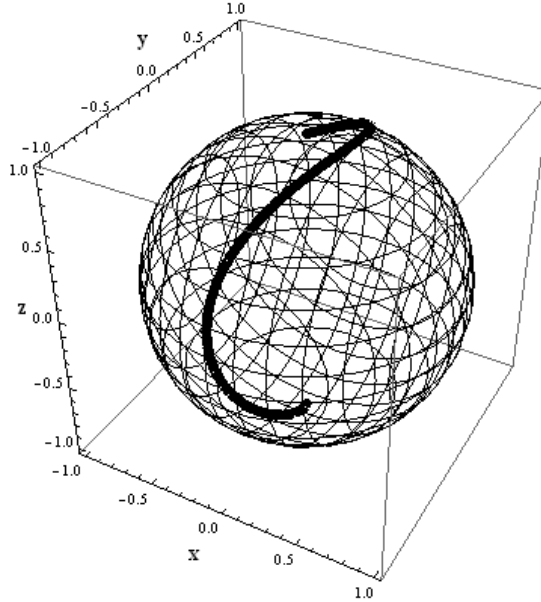


FIG. 2: Illustrative depiction of the nongeodesic evolution path (thick solid line) on the Bloch sphere generated by the nonstationary Hamiltonian $H(t)$ associated to a phase $\beta(t)$ that exhibits exponential growth. The evolution occurs from $|A\rangle \stackrel{\text{def}}{=} |0\rangle$ to $|B\rangle \stackrel{\text{def}}{=} |1\rangle$. For simplicity, we set $\nu_0 = \omega_0 = 1$ and $0 \leq t \leq \pi/2$. Physical units are chosen using $\hbar = 1$.

expression for η_{GE} . However, it can be numerically estimated for a given choice of ω_0 and ν_0 . For example, setting $\omega_0 = \nu_0 = 1$, we find $s \simeq 3.27 \geq \pi = s_0$. In analogy to the first two examples, the magnetic field vector $\mathbf{h}(t)$ possesses no longitudinal vector component and, in addition, is fully transverse since $\mathbf{h}(t) = \mathbf{h}_\perp(t)$. Similarly to the second example, $h_\perp(t) = \sqrt{\mathbf{h}_\perp \cdot \mathbf{h}_\perp}$ is time-varying. In particular, we have $h_\perp(t) = \sqrt{\omega_0^2 + (1/4)\nu_0^4 t^2 \sin^2(2\omega_0 t)}$.

Speed efficiency. From the perspective of speed efficiency, the evolution occurs with $\eta_{\text{SE}}(t) = 1$ for any $0 \leq t \leq \pi/(2\omega_0)$. Similar to the first two examples, this is due to the functional structure of the Hamiltonian $H(t)$. Furthermore, the unit speed efficiency can also be elucidated by the absence of the longitudinal vector component (i.e., $\mathbf{h}_\parallel(t) = \mathbf{0}$) of the magnetic field vector $\mathbf{h}(t)$.

Curvature. In analogy to what happens in the second application, the curvature coefficient κ_{AC}^2 of this third quantum evolution does not vanish. This agrees with the inequality $\eta_{\text{GE}} < 1$. After some algebraic manipulations, κ_{AC}^2 in Eq. (12) reduces to

$$[\kappa_{\text{AC}}^2(t; \omega_0, \nu_0)]_{\text{Example-3}} = \frac{\mathbf{h}^2(t; \omega_0, \nu_0) \dot{\mathbf{h}}^2(t; \omega_0, \nu_0) - [\mathbf{h}(t; \omega_0, \nu_0) \cdot \dot{\mathbf{h}}(t; \omega_0, \nu_0)]^2}{\mathbf{h}^6(t; \omega_0, \nu_0)}, \quad (42)$$

where \mathbf{h}^2 , $\dot{\mathbf{h}}^2$, and $(\mathbf{h} \cdot \dot{\mathbf{h}})^2$ in Eq. (42) are given by

$$\begin{aligned} \mathbf{h}^2 &\stackrel{\text{def}}{=} \omega_0^2 + \frac{1}{4}\nu_0^4 t^2 \sin^2(2\omega_0 t), \\ \dot{\mathbf{h}}^2 &\stackrel{\text{def}}{=} \frac{1}{16}\nu_0^8 t^4 \sin^2(4\omega_0 t) + \frac{1}{4}\nu_0^4 \sin^2(2\omega_0 t) + 2\nu_0^4 \omega_0^2 t^2 [1 + \cos(4\omega_0 t)] + \nu_0^4 \omega_0 t \sin(4\omega_0 t), \\ \mathbf{h} \cdot \dot{\mathbf{h}} &\stackrel{\text{def}}{=} \frac{1}{4}\nu_0^4 t [\omega_0 t \sin(4\omega_0 t) + \sin^2(2\omega_0 t)], \end{aligned} \quad (43)$$

respectively. As a supplementary remark, we note that the short-time limit of $[\kappa_{\text{AC}}^2(t; \omega_0, \nu_0)]_{\text{Example-3}}$ is represented as

$$[\kappa_{\text{AC}}^2(t; \omega_0, \nu_0)]_{\text{Example-3}} \xrightarrow{t \rightarrow 0} 9\nu_0^2 \left(\frac{\nu_0}{\omega_0}\right)^2 t^2 - 28\nu_0^4 t^4 + \mathcal{O}(t^5), \quad (44)$$

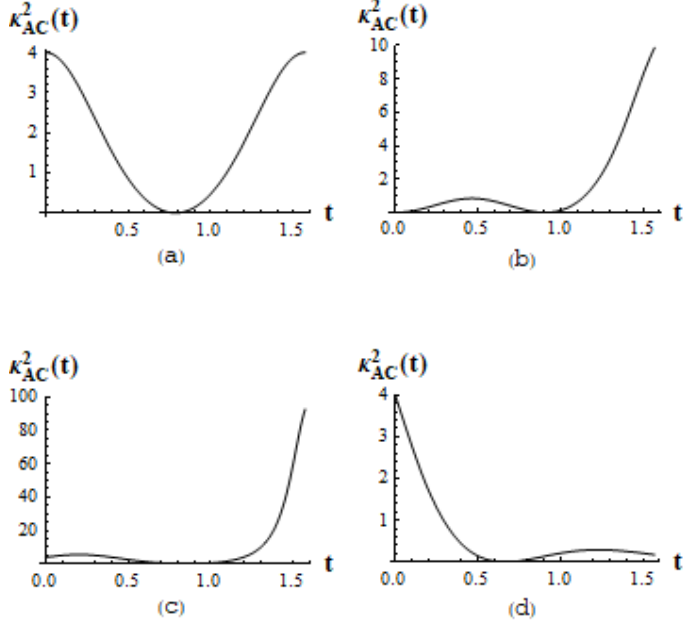


FIG. 3: Temporal behavior of the curvature coefficient $\kappa_{AC}^2(t)$ of the quantum evolution when the phase $\beta(t)$ exhibits linear growth (a), quadratic growth (b), exponential growth (c) and, finally, exponential decay (d). In all plots, we set $\nu_0 = \omega_0 = 1$ and $0 \leq t \leq \pi/2$. Physical units are chosen using $\hbar = 1$.

where $[\kappa_{AC}^2(t; \omega_0, \nu_0)]_{\text{Example-3}}$ starts at a value of zero when $t = 0$. Finally, the existence of a non-zero curvature coefficient arises from the fact that $\mathbf{h}(t)$ and $\dot{\mathbf{h}}(t)$ are not collinear (i.e., $\partial_t \dot{\mathbf{h}}(t) \neq \mathbf{0}$, with $\mathbf{h}(t) = h(t)\dot{\mathbf{h}}(t)$). In other words, contrary to the situation that occurs in the first example, the magnetic field varies in both magnitude and direction.

Complexity. Finally, from a complexity perspective, we observe that $\theta(t) = 2\omega_0 t$ and $\varphi(t) = (1/2)\nu_0^2 t^2$, with $0 \leq \theta \leq \pi$, $0 \leq \varphi \leq (\pi/2)[(\pi/2)(\nu_0/\omega_0)]^2$, and $0 \leq t \leq \pi/(2\omega_0)$. Therefore, a straightforward computation leads to expressions for the instantaneous, accessed, and accessible volumes given by

$$V(t) = \frac{\nu_0^2}{8} [1 - \cos(2\omega_0 t)] t^2, \quad \bar{V} = \left(\frac{1}{16} + \frac{\pi^2}{96} \right) \left(\frac{\nu_0}{\omega_0} \right)^2, \quad \text{and} \quad V_{\max} = \frac{\pi^2}{16} \left(\frac{\nu_0}{\omega_0} \right)^2, \quad (45)$$

respectively. Lastly, the complexity of this quantum evolution becomes

$$C = \frac{5\pi^2 - 6}{6\pi^2}. \quad (46)$$

Intriguingly, we emphasize that $[C]_{\text{Example-3}}$ in Eq. (46) is approximately equal to 0.73 and is greater than both $[C]_{\text{Example-2}} \simeq 0.65$ and $[C]_{\text{Example-1}} = 0.5$. Importantly, the observation that in the quadratic growth scenario, the complexity C in Eq. (46) attains a constant value that is independent of the parameters ω_0 and ν_0 stems from the fact that both \bar{V} and V_{\max} are proportional to the ratio $(\nu_0/\omega_0)^2$.

D. Exponential growth

In the fourth example, we suppose that $\mathbf{h}(t)$ is described by a phase $\beta(t)$ that grows exponentially in time. Specifically, we put $\beta(t) \stackrel{\text{def}}{=} e^{\nu_0 t}$ with $\nu_0 \in \mathbb{R}_+ \setminus \{0\}$ so that $\dot{\beta} = \nu_0 e^{\nu_0 t}$. Keeping in mind that $\alpha(t) = \omega_0 t$, the evolution we investigate happens from $|A\rangle = |0\rangle$ to $|B\rangle \simeq |1\rangle$ in a temporal interval $t_{\text{final}} = \pi/(2\omega_0)$. In Figure 2, we depict the non-geodesic evolution trajectory on the Bloch sphere produced by the nonstationary Hamiltonian, which is linked to a phase that demonstrates exponential growth.

Geodesic efficiency. From a geodesic efficiency perspective, we observe that the geodesic distance s_0 from $|A\rangle$ to $|B\rangle$ equals $s_0 = \pi$. Moreover, the energy uncertainty $\Delta E(t) = \sqrt{\langle \dot{m} | \dot{m} \rangle}$ varies in time since $\langle \dot{m} | \dot{m} \rangle = \dot{\alpha}^2 + (1/4)\dot{\beta}^2 \sin^2(2\alpha)$ yields $\Delta E^2(t) = \omega_0^2 + (1/4)\nu_0^2 e^{2\nu_0 t} \sin^2(2\omega_0 t)$. As a consequence, the quantum evolution in this fourth case exhibits a geodesic efficiency $\eta_{GE} < 1$ since $s > s_0 = \pi$. In analogy to the last two examples, the efficiency η_{GE} is a function of ω_0 and ν_0 . Although there is no useful closed form expression for η_{GE} , one can numerically evaluate it for a suitable choice of values for ω_0 and ν_0 . For instance, letting $\omega_0 = \nu_0 = 1$, we find $s \simeq 4.04 \geq \pi = s_0$. Analogously to the first three examples, the magnetic field vector $\mathbf{h}(t)$ is completely transverse (i.e., $\mathbf{h}(t) = \mathbf{h}_\perp(t)$) and exhibits no longitudinal vector component (i.e., $\mathbf{h}_\parallel = \mathbf{0}$). In analogy to the second and third examples, $h_\perp(t) = \sqrt{\mathbf{h}_\perp \cdot \mathbf{h}_\perp}$ is nonstationary. In particular, we have $h_\perp(t) = \sqrt{\omega_0^2 + (1/4)\nu_0^2 e^{2\nu_0 t} \sin^2(2\omega_0 t)}$.

Speed efficiency. From the viewpoint of speed efficiency, the evolution is characterized by $\eta_{SE}(t) = 1$ for any $0 \leq t \leq \pi/(2\omega_0)$. In a manner akin to the first three examples, this phenomenon arises from the functional structure of the Hamiltonian $H(t)$. Additionally, the unit speed efficiency can be further clarified by the lack of the longitudinal vector component (i.e., $\mathbf{h}_\parallel(t) = \mathbf{0}$) of the magnetic field vector $\mathbf{h}(t)$.

Curvature. In a manner similar to the events occurring in the second and third applications, the curvature coefficient κ_{AC}^2 associated with this fourth quantum evolution does not become zero. This is consistent with the inequality $\eta_{GE} < 1$. Following a series of algebraic manipulations, κ_{AC}^2 in Eq. (12) simplifies to

$$[\kappa_{AC}^2(t; \omega_0, \nu_0)]_{\text{Example-4}} = \frac{\mathbf{h}^2(t; \omega_0, \nu_0) \dot{\mathbf{h}}^2(t; \omega_0, \nu_0) - [\mathbf{h}(t; \omega_0, \nu_0) \cdot \dot{\mathbf{h}}(t; \omega_0, \nu_0)]^2}{\mathbf{h}^6(t; \omega_0, \nu_0)}, \quad (47)$$

with \mathbf{h}^2 , $\dot{\mathbf{h}}^2$, and $(\mathbf{h} \cdot \dot{\mathbf{h}})^2$ in Eq. (47) being defined as

$$\begin{aligned} \mathbf{h}^2 &\stackrel{\text{def}}{=} \omega_0^2 + \frac{1}{4}\nu_0^2 e^{2\nu_0 t} \sin^2(2\omega_0 t), \\ \dot{\mathbf{h}}^2 &\stackrel{\text{def}}{=} \frac{1}{16}\nu_0^2 e^{2t\nu_0} \{4\nu_0^2 \sin^2(2\omega_0 t) + 32\omega_0^2 [1 + \cos(4\omega_0 t)] + \nu_0^2 e^{2t\nu_0} \sin^2(4\omega_0 t) + 16\nu_0 \omega_0 \sin(4\omega_0 t)\}, \\ \mathbf{h} \cdot \dot{\mathbf{h}} &\stackrel{\text{def}}{=} \frac{1}{4}\nu_0^2 e^{2t\nu_0} [\nu_0 \sin^2(2\omega_0 t) + \omega_0 \sin(4\omega_0 t)], \end{aligned} \quad (48)$$

respectively. As an additional observation, we observe that the short-time limit of $[\kappa_{AC}^2(t; \omega_0, \nu_0)]_{\text{Example-4}}$ is articulated as

$$[\kappa_{AC}^2(t; \omega_0, \nu_0)]_{\text{Example-4}} \xrightarrow{t \rightarrow 0} 4 \left(\frac{\nu_0}{\omega_0} \right)^2 + 12\nu_0 \left(\frac{\nu_0}{\omega_0} \right)^2 t + \left(\frac{\nu_0}{\omega_0} \right)^2 (9\nu_0^2 - 16\omega_0^2) t^2 + \mathcal{O}(t^3), \quad (49)$$

where $[\kappa_{AC}^2(t; \omega_0, \nu_0)]_{\text{Example-4}}$ initiates at the nonzero value of $4(\nu_0/\omega_0)^2$ at $t = 0$. Lastly, the presence of a non-zero curvature coefficient is due to the non-collinearity of $\mathbf{h}(t)$ and $\dot{\mathbf{h}}(t)$ (i.e., $\partial_t \dot{\mathbf{h}}(t) \neq \mathbf{0}$, with $\mathbf{h}(t) = h(t)\dot{\mathbf{h}}(t)$). In contrast to the scenario presented in the first example (and, in addition, similarly to the second and third cases), the magnetic field exhibits variations in both its magnitude and direction.

Complexity. Lastly, from a complexity standpoint, we note that $\theta(t) = 2\omega_0 t$ and $\varphi(t) = e^{\nu_0 t}$, with $0 \leq \theta \leq \pi$, $1 \leq \varphi \leq e^{\frac{\pi}{2}\frac{\nu_0}{\omega_0}}$, and $0 \leq t \leq \pi/(2\omega_0)$. Consequently, a simple calculation results in formulas for the instantaneous, accessed, and accessible volumes expressed as

$$V(t) = \frac{[1 - \cos(2\omega_0 t)] (e^{\nu_0 t} - 1)}{4}, \quad \bar{V} = \bar{V} \left(\frac{\nu_0}{\omega_0} \right) \stackrel{\text{def}}{=} \frac{\left[\left(\frac{\nu_0}{\omega_0} \right)^2 + 2 \right] e^{\frac{\pi}{2}\frac{\nu_0}{\omega_0}} - 2}{\pi \left(\frac{\nu_0}{\omega_0} \right) \left[\left(\frac{\nu_0}{\omega_0} \right)^2 + 4 \right]} - \frac{1}{4}, \quad \text{and} \quad V_{\max} = V_{\max} \left(\frac{\nu_0}{\omega_0} \right) \stackrel{\text{def}}{=} \frac{e^{\frac{\pi}{2}\frac{\nu_0}{\omega_0}} - 1}{2}, \quad (50)$$

respectively. Finally, the complexity of this fourth quantum evolution becomes

$$C = C \left(\frac{\nu_0}{\omega_0} \right) \stackrel{\text{def}}{=} \frac{\left[2\pi \left(\frac{\nu_0}{\omega_0} \right)^3 - 4 \left(\frac{\nu_0}{\omega_0} \right)^2 + 8\pi \frac{\nu_0}{\omega_0} - 8 \right] e^{\frac{\pi}{2}\frac{\nu_0}{\omega_0}} - \left[\pi \left(\frac{\nu_0}{\omega_0} \right)^3 + 4\pi \frac{\nu_0}{\omega_0} - 8 \right]}{\left[2\pi \left(\frac{\nu_0}{\omega_0} \right)^3 + 8\pi \frac{\nu_0}{\omega_0} \right] e^{\frac{\pi}{2}\frac{\nu_0}{\omega_0}} - \left[2\pi \left(\frac{\nu_0}{\omega_0} \right)^3 + 8\pi \frac{\nu_0}{\omega_0} \right]}. \quad (51)$$

Unlike what we found in the previous three examples, $[C]_{\text{Example-4}} = C(\omega_0, \nu_0)$ in Eq. (51) does not assume a constant value, regardless of any choice of ω_0 and ν_0 . The behavior of $C(\omega_0, \nu_0)$ is more complicated. This complication arises from the fact that \bar{V} and V_{\max} demonstrate a dependence on ω_0 and ν_0 that cannot be encapsulated by a universal scaling factor of the form $(\nu_0/\omega_0)^n$ with $n \in \mathbb{N}$, for example. Technical details on the derivation of Eq. (51) along with a discussion of the limiting cases in which ν_0/ω_0 approaches zero or infinity are located in Appendix D.

E. Exponential decay

In this last example, we assume that $\mathbf{h}(t)$ is characterized by a phase $\beta(t)$ that decays exponentially in time. In particular, we set $\beta(t) \stackrel{\text{def}}{=} e^{-\nu_0 t}$ with $\nu_0 \in \mathbb{R}_+ \setminus \{0\}$ so that $\dot{\beta} = -\nu_0 e^{-\nu_0 t}$. Given that $\alpha(t) = \omega_0 t$, the evolution we consider propagates from $|A\rangle = |0\rangle$ to $|B\rangle \simeq |1\rangle$ in a time span specified by $t_{\text{final}} = \pi/(2\omega_0)$.

Geodesic efficiency. From a geodesic efficiency viewpoint, we note that the geodesic distance s_0 from $|A\rangle$ to $|B\rangle$ is $s_0 = \pi$. Additionally, the energy uncertainty $\Delta E(t) = \sqrt{\langle \dot{m} | \dot{m} \rangle}$ does not remain constant in time because $\langle \dot{m} | \dot{m} \rangle = \dot{\alpha}^2 + (1/4)\dot{\beta}^2 \sin^2(2\alpha)$ leads to $\Delta E^2(t) = \omega_0^2 + (1/4)\nu_0^2 e^{-2\nu_0 t} \sin^2(2\omega_0 t)$. Therefore, the quantum-mechanical evolution in this last scenario shows a geodesic efficiency $\eta_{\text{GE}} < 1$ given that $s > s_0 = \pi$. Analogously to the last three examples, the efficiency η_{GE} depends on ω_0 and ν_0 . Again, even though there is not any convenient closed form formula for η_{GE} , it is possible to numerically calculate it for a given choice of values for ω_0 and ν_0 . For example, setting $\omega_0 = \nu_0 = 1$, we obtain $s \simeq 3.19 \geq \pi = s_0$. In analogy to the first four examples, the magnetic field vector $\mathbf{h}(t)$ exhibits a fully transverse vector component (i.e., $\mathbf{h}(t) = \mathbf{h}_{\perp}(t)$) and does not possess any longitudinal vector component (i.e., $\mathbf{h}_{\parallel} = \mathbf{0}$). Furthermore, $h_{\perp}(t) = \sqrt{\mathbf{h}_{\perp} \cdot \mathbf{h}_{\perp}}$ is time-varying, with $h_{\perp}(t) = \sqrt{\omega_0^2 + (1/4)\nu_0^2 e^{-2\nu_0 t} \sin^2(2\omega_0 t)}$.

Speed efficiency. From the perspective of speed efficiency, the evolution is defined by $\eta_{\text{SE}}(t) = 1$ for any $0 \leq t \leq \pi/(2\omega_0)$. Similar to the previous four examples, this occurrence stems from the functional framework of the Hamiltonian $H(t)$. Furthermore, the unit speed efficiency can be elucidated by the absence of the longitudinal vector component (i.e., $\mathbf{h}_{\parallel}(t) = \mathbf{0}$) of the magnetic field vector $\mathbf{h}(t)$.

Curvature. In a manner akin to the occurrences in the second, third, and fourth applications, the curvature coefficient κ_{AC}^2 related to this fifth quantum evolution does not reach zero. This aligns with the inequality $\eta_{\text{GE}} < 1$. After performing a sequence of algebraic calculations, κ_{AC}^2 in Eq. (12) is simplified to

$$[\kappa_{\text{AC}}^2(t; \omega_0, \nu_0)]_{\text{Example-5}} = \frac{\mathbf{h}^2(t; \omega_0, \nu_0) \dot{\mathbf{h}}^2(t; \omega_0, \nu_0) - [\mathbf{h}(t; \omega_0, \nu_0) \cdot \dot{\mathbf{h}}(t; \omega_0, \nu_0)]^2}{\mathbf{h}^6(t; \omega_0, \nu_0)}, \quad (52)$$

where \mathbf{h}^2 , $\dot{\mathbf{h}}^2$, and $(\mathbf{h} \cdot \dot{\mathbf{h}})^2$ in Eq. (52) are given by

$$\begin{aligned} \mathbf{h}^2 &\stackrel{\text{def}}{=} \omega_0^2 + \frac{1}{4}\nu_0^2 e^{-2\nu_0 t} \sin^2(2\omega_0 t), \\ \dot{\mathbf{h}}^2 &\stackrel{\text{def}}{=} \frac{1}{16}\nu_0^2 e^{-2\nu_0 t} \{4\nu_0^2 \sin^2(2\omega_0 t) + 32\omega_0^2 [1 + \cos(4\omega_0 t)] + \nu_0^2 e^{-2\nu_0 t} \sin^2(4\omega_0 t) - 16\nu_0 \omega_0 \sin(4\omega_0 t)\}, \\ \mathbf{h} \cdot \dot{\mathbf{h}} &\stackrel{\text{def}}{=} \frac{1}{4}\nu_0^2 e^{-2\nu_0 t} [\omega_0 \sin(4\omega_0 t) - \nu_0 \sin^2(2\omega_0 t)], \end{aligned} \quad (53)$$

respectively. As a side note, we observe that the short-time limit of $[\kappa_{\text{AC}}^2(t; \omega_0, \nu_0)]_{\text{Example-5}}$ is represented by

$$[\kappa_{\text{AC}}^2(t; \omega_0, \nu_0)]_{\text{Example-5}} \stackrel{t \rightarrow 0}{\simeq} 4 \left(\frac{\nu_0}{\omega_0} \right)^2 - 12\nu_0 \left(\frac{\nu_0}{\omega_0} \right)^2 t + \left(\frac{\nu_0}{\omega_0} \right)^2 (9\nu_0^2 - 16\omega_0^2) t^2 + \mathcal{O}(t^3), \quad (54)$$

where $[\kappa_{\text{AC}}^2(t; \omega_0, \nu_0)]_{\text{Example-5}}$ begins at the nonzero value of $4(\nu_0/\omega_0)^2$ at $t = 0$. Finally, the existence of a non-zero curvature coefficient arises from the non-collinearity of $\mathbf{h}(t)$ and $\dot{\mathbf{h}}(t)$ (i.e., $\partial_t \hat{h}(t) \neq \mathbf{0}$, with $\mathbf{h}(t) = h(t)\hat{h}(t)$). Unlike the situation described in the first example (and similarly to the second, third, and fourth examples), the magnetic field shows fluctuations in both its magnitude and direction.

Complexity. Finally, from a complexity perspective, we remark that $\theta(t) = 2\omega_0 t$ and $\varphi(t) = e^{-\nu_0 t}$, with $0 \leq \theta \leq \pi$, $e^{-\frac{\pi}{2}\frac{\nu_0}{\omega_0}} \leq \varphi \leq 1$, and $0 \leq t \leq \pi/(2\omega_0)$. Therefore, a straightforward computation yields expressions for the

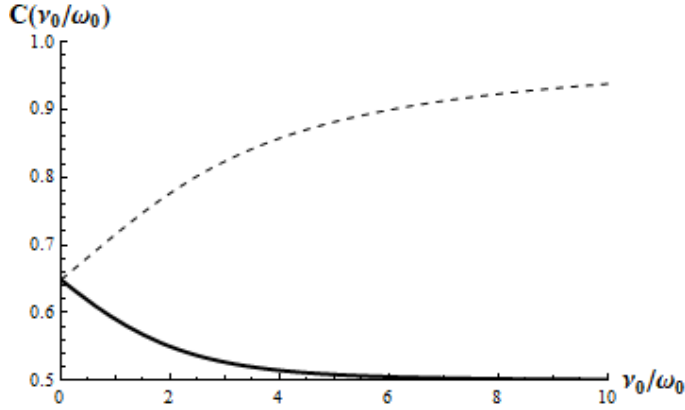


FIG. 4: Behavior of the complexity of the quantum evolution specified by the nonstationary Hamiltonian $H(t)$ corresponding to the phase $\beta(t)$ that grows exponentially (dashed line) or decays exponentially (thick solid line). The complexity C is plotted versus the ratio ν_0/ω_0 . When $\nu_0/\omega_0 \gg 1$ and $\beta(t)$ grows exponentially, the complexity asymptotically approaches its maximum value 1. Alternatively, when $\nu_0/\omega_0 \gg 1$ and $\beta(t)$ decays exponentially, the complexity asymptotically approaches the limiting value of 1/2, that is to say the complexity value that characterizes the geodesic evolution on the Bloch sphere between initial and final states $|A\rangle \stackrel{\text{def}}{=} |0\rangle$ and $|B\rangle \stackrel{\text{def}}{=} |1\rangle$, respectively.

instantaneous, accessed, and accessible volumes given by

$$V(t) = \frac{[1 - \cos(2\omega_0 t)](1 - e^{-\nu_0 t})}{4}, \bar{V} = \bar{V}\left(\frac{\nu_0}{\omega_0}\right) \stackrel{\text{def}}{=} \frac{1}{4} - \frac{2 - \left[\left(\frac{\nu_0}{\omega_0}\right)^2 + 2\right]e^{-\frac{\pi}{2}\frac{\nu_0}{\omega_0}}}{\pi\left(\frac{\nu_0}{\omega_0}\right)\left[\left(\frac{\nu_0}{\omega_0}\right)^2 + 4\right]}, \text{ and } V_{\max} = V_{\max}\left(\frac{\nu_0}{\omega_0}\right) \stackrel{\text{def}}{=} \frac{1 - e^{-\frac{\pi}{2}\frac{\nu_0}{\omega_0}}}{2}, \quad (55)$$

respectively. Lastly, the complexity of this last quantum evolution reduces to

$$C = C\left(\frac{\nu_0}{\omega_0}\right) \stackrel{\text{def}}{=} \frac{\left[\pi\left(\frac{\nu_0}{\omega_0}\right)^3 + 4\pi\left(\frac{\nu_0}{\omega_0}\right) + 8\right]e^{\frac{\pi}{2}\frac{\nu_0}{\omega_0}} - \left[2\pi\left(\frac{\nu_0}{\omega_0}\right)^3 + 4\left(\frac{\nu_0}{\omega_0}\right)^2 + 8\pi\left(\frac{\nu_0}{\omega_0}\right) + 8\right]}{\left[2\pi\left(\frac{\nu_0}{\omega_0}\right)^3 + 8\pi\left(\frac{\nu_0}{\omega_0}\right)\right]e^{\frac{\pi}{2}\frac{\nu_0}{\omega_0}} - \left[2\pi\left(\frac{\nu_0}{\omega_0}\right)^3 + 8\pi\left(\frac{\nu_0}{\omega_0}\right)\right]}. \quad (56)$$

Like what we find in the fourth example, $[C]_{\text{Example-5}} = C(\omega_0, \nu_0)$ in Eq. (56) is not constant in ω_0 and ν_0 . The parametric behavior of $C(\omega_0, \nu_0)$ is more intricate. This intricacy arises from the fact that \bar{V} and V_{\max} show a dependence on ω_0 and ν_0 that cannot be expressed, for instance, through a common scaling factor of the form $(\nu_0/\omega_0)^n$ with $n \in \mathbb{N}$, for example. Technical details on the derivation of Eq. (56) along with a discussion of the limiting cases in which ν_0/ω_0 approaches zero or infinity are located in Appendix A. In Fig. 3, we show the temporal behavior of the curvature coefficient of the the various quantum evolutions considered here. Finally, we present in Fig. 4 the parametric characteristics of the complexity of quantum evolution defined by the nonstationary Hamiltonian, which corresponds to the phase $\beta(t)$ in $|\psi(t)\rangle = \cos(\omega_0 t)|0\rangle + e^{i\beta(t)}\sin(\omega_0 t)|1\rangle$ (see Eq. (29)) that either increases exponentially or decreases exponentially.

VI. FINAL REMARKS

In this paper, we presented a geometric characterization of nonstationary Hamiltonian evolutions in two-level quantum systems (Eq. (28) and Fig. 1), with special concern on efficiency (Eqs. (1) and (5)), curvature (12), and complexity (13) of quantum evolutions (Fig. 2). In particular, we reported exact analytical expressions for the curvature of quantum evolutions related to a two-level quantum system influenced by a variety of time-dependent magnetic field configurations (Eqs. (37), (42), (47), and (52)). More specifically, we investigated the dynamics generated by a two-parameter nonstationary Hermitian Hamiltonian operating at unit speed efficiency. To deepen our comprehension of the physical implications of the curvature coefficient, we scrutinized the curvature behavior (Fig. 3) in connection with geodesic efficiency, speed efficiency, and the complexity of the quantum evolution. Our

results suggest that, in general, efficient quantum evolutions tend to exhibit lower complexity than their inefficient counterparts (Table I and Fig. 4). Nevertheless, it is important to highlight that complexity is not solely determined by length. Indeed, longer paths that are sufficiently curved may reveal a complexity that is less than that of shorter paths characterized by a lower curvature coefficient. For instance, considering our second (linear growth, Eq. (41)) and third (quadratic growth, Eq. (46)) examples, we have that $[C]_{\text{Example-2}} \simeq 0.65 \leq 0.73 \simeq [C]_{\text{Example-3}}$ does not generally imply that $[s(\nu_0, \omega_0)]_{\text{Example-2}} \leq [s(\nu_0, \omega_0)]_{\text{Example-3}}$ (with s defined in Eq. (1)). Indeed, after some algebra, it happens that for $\nu_0/\omega_0 \leq 2/\pi$, $[s(\nu_0, \omega_0)]_{\text{Example-2}} \geq [s(\nu_0, \omega_0)]_{\text{Example-3}}$. For instance, setting $\nu_0 = 1$ [MKSA] and $\omega_0 = 5$ [MKSA], one arrives at $[s(1, 5)]_{\text{Example-2}} \simeq 1.575 \geq 1.571 \simeq [s(1, 5)]_{\text{Example-3}}$. In addition, $[\kappa_{\text{AC}}^2(t)]_{\text{Example-2}} \geq [\kappa_{\text{AC}}^2(t)]_{\text{Example-3}}$ with $0 \leq t \leq \pi/(2\omega_0)$ and $\omega_0 = 5$ [MKSA]. These considerations, arising here from nonstationary Hamiltonian evolutions, align with those documented in a time-independent Hamiltonian context as referenced in Ref. [34].

To summarize, our principal findings can be articulated as follows:

- [i] We developed a two-parameter family of nonstationary Hamiltonians (Eq. (28)) that produce analytically solvable Schrödinger evolution trajectories. Notably, the two parameters (i.e., $\alpha(t)$ and $\beta(t)$) can be interpreted as adjustable parameters that define the time-varying magnetic field vector, which characterizes the traceless nonstationary Hamiltonian, or alternatively, the polar and azimuthal angles (i.e., $\theta(t)$ and $\varphi(t)$) utilized to parametrize the evolving state vectors of the Bloch sphere.
- [ii] For the first time in the literature (to the best of our knowledge), we conducted a geometrically-driven comparative analysis of various dynamical paths on the Bloch sphere that correspond to different time-varying Hamiltonian models. Each trajectory was defined in terms of geodesic and speed efficiencies (Eqs. (1) and (5)), curvature coefficient (Eq. (12)), and ultimately, complexity of the corresponding quantum evolution (Eq. (13)).
- [iii] We demonstrated the significance of relative phase factors in quantum dynamics by examining the short-time behavior of the curvature coefficient across various quantum evolutions, adjusting the time-dependent phase $\beta(t)$ that appears in the relative phase factor $e^{i\beta(t)}$ (and, in addition, in the magnetic field vector \mathbf{h} in Eq. (34)) that defines the evolving state vector of interest (Eqs. (29) and (32)). Variations in phases not only affect the length of the trajectory but also influence the manner in which the trajectory curves as it connects the initial and final states.
- [iv] Changes in lengths and curvature serve as indicators of alterations in the complexity of the dynamical evolution. Indeed, we illustrated how these variations are reflected in the accessed and accessible volumes of the parametric regions on the Bloch sphere (Eqs. (41), (46), (51), and (56)) that arise from the different nonstationary Hamiltonian models under investigation.

In our opinion, this paper represents a notable progress in relation to our recent works appeared in Refs. [16, 35]. Indeed, in contrast to Ref. [16], we have broadened our investigation to encompass the curvature of quantum evolutions across various time-dependent magnetic field configurations, thus covering a diverse range of typical temporal profiles. Additionally, unlike Ref. [16], we have examined the temporal behavior of the curvature coefficients and established a connection to the complexity of the different quantum evolutions. Lastly, in contrast to Ref. [35], we have expanded our analysis to include the complexity of quantum evolutions characterized by non-stationary Hamiltonians. To the best of our understanding, most curvature analyses of quantum evolutions documented in the literature are confined to time-independent contexts [12, 44–47]. Furthermore, the majority of studies based on Krylov state complexity concentrate on time-independent Hamiltonian evolutions, with the extension to a completely nonstationary framework still in its nascent phase [48, 49]. For these reasons, the findings we present here are even more significant.

Despite these considerable advancements, several limitations and potential improvements deserve consideration. From the perspective of curvature analysis, one might focus on examining the temporal profiles of magnetic fields that could more closely resemble actual physical realizations within a quantum laboratory. Nevertheless, one of the significant challenges in this regard is the difficulty in acquiring precise analytical solutions to the time-dependent Schrödinger equation [50–58]. Furthermore, although the formula for κ_{AC}^2 is theoretically applicable to any d -level quantum system evolving under a nonstationary Hamiltonian, our investigation was limited to systems comprising only two levels. In this simpler context, the comprehension and visual depiction of Bloch vectors and Bloch spheres are relatively straightforward, in contrast to more intricate, higher-dimensional scenarios. As we transition from systems with merely two levels to those with additional dimensions, the clarity of these visual representations diminishes. Indeed, quantum theory reveals distinctive features in more complex systems, including the simplest yet non-trivial case involving three levels, referred to as qutrits [59]. These unusual quantum phenomena complicate the understanding of the geometric structure of quantum systems in higher dimensions [60, 61]. We suggest consulting Ref. [62] for a

thorough overview of how Bloch vectors are utilized to represent single-qubit, single-qutrit, and two-qubit systems, employing matrices such as Pauli, Gell-Mann, and Dirac matrices, respectively. From a complexity analysis perspective, although we have proposed our own method for quantifying the complexity of quantum evolutions, it is crucial to recognize the established methodologies available in the literature, as noted in the Introduction. A significant approach is the one based on Krylov complexity [17, 18, 24, 27, 63–68]. This complexity measure serves as a vital metric for assessing the rate at which quantum states propagate over time within the Krylov space derived from the initial state or, alternatively, the speed at which operators disseminate across the entire spectrum of potential operators during dynamic evolution. It is anticipated that the late-time plateau of this metric will aid in differentiating between integrable and chaotic dynamics; however, its effectiveness in this regard is significantly influenced by the selection of the initial seed [68, 69]. It would be valuable to conduct a thorough comparative analysis between our complexity measure and the Krylov state complexity in both stationary and nonstationary qubit dynamics contexts. Nevertheless, this matter falls outside the current scope, and for now, we shall postpone this intriguing inquiry to future scientific pursuits.

To sum up, even though it has its present constraints, we truly believe that our research will encourage other researchers and set the stage for more in-depth studies on how geometry and quantum mechanics interact.

ACKNOWLEDGMENTS

C.C. is grateful to the Griffiss Institute (Rome-NY) and to the United States Air Force Research Laboratory (AFRL) Visiting Faculty Research Program (VFRP) for providing support for this work. J.S. acknowledges support from the AFRL. The authors appreciate the insightful conversations conducted with P. M. Alsing. Any opinions, findings and conclusions or recommendations expressed in this material are those of the authors and do not necessarily reflect the views of the AFRL.

-
- [1] R. P. Feynman, F. Vernon, and R. W. Hellwarth, *Geometrical representation of the Schrödinger equation for solving maser problems*, J. Appl. Phys. **28**, 49 (1957).
 - [2] C. M. Bender, D. C. Brody, H. F. Jones, and B. K. Meister, *Faster than Hermitian quantum mechanics*, Phys. Rev. Lett. **98**, 040403 (2007).
 - [3] C. M. Bender and D. C. Brody, *Optimal time evolution for Hermitian and non-Hermitian Hamiltonians*, Lecture Notes in Physics **789**, 341 (2009).
 - [4] A. Mostafazadeh, *Hamiltonians generating optimal-speed evolutions*, Phys. Rev. **A79**, 014101 (2009).
 - [5] C. Cafaro and P. M. Alsing, *Qubit geodesics on the Bloch sphere from optimal-speed Hamiltonian evolutions*, Class. Quantum Grav. **40**, 115005 (2023).
 - [6] B. Hetenyi and P. Levay, *Fluctuations, uncertainty relations, and the geometry of quantum state manifolds*, Phys. Rev. **A108**, 032218 (2023).
 - [7] C. Chryssomalakos et al., *Curves in quantum state space, geometric phases, and the brachistophase*, J. Phys. A: Math. Theor. **56**, 285301 (2023).
 - [8] C. Chryssomalakos et al., *Speed excess and total acceleration: A kinematical approach to entanglement*, Phys. Scr. **99**, 125116 (2024).
 - [9] J. Anandan and Y. Aharonov, *Geometry of quantum evolution*, Phys. Rev. Lett. **65**, 1697 (1990).
 - [10] D. B. Brody and L. P. Hughston, *Geometry of quantum statistical inference*, Phys. Rev. Lett. **77**, 2851 (1996).
 - [11] D. C. Brody and Eva-Marie Graefe, *Information geometry of complex Hamiltonians and exceptional points*, Entropy **15**, 3361 (2013).
 - [12] H. P. Laba and V. M. Tkachuk, *Geometric characteristics of quantum evolution: Curvature and torsion*, Condensed Matter Physics **20**, 13003 (2017).
 - [13] P. M. Alsing and C. Cafaro, *From the classical Frenet–Serret apparatus to the curvature and torsion of quantum-mechanical evolutions. Part I. Stationary Hamiltonians*, Int. J. Geom. Methods Mod. Phys. **21**, 2450152 (2024).
 - [14] P. M. Alsing and C. Cafaro, *From the classical Frenet–Serret apparatus to the curvature and torsion of quantum-mechanical evolutions. Part II. Nonstationary Hamiltonians*, Int. J. Geom. Methods Mod. Phys. **21**, 2450151 (2024).
 - [15] P. M. Alsing and C. Cafaro, *Upper limit on the acceleration of a quantum evolution in projective Hilbert space*, Int. J. Geom. Methods Mod. Phys. **21**, 2440009 (2024).
 - [16] C. Cafaro, L. Rossetti, and P. M. Alsing, *Curvature of quantum evolutions for qubits in time-dependent magnetic fields*, Phys. Rev. **A111**, 012408 (2025).
 - [17] S. Chapman, M. P. Heller, H. Marrochio, and F. Pastawski, *Toward a definition of complexity for quantum field theory states*, Phys. Rev. Lett. **120**, 121602 (2018).
 - [18] J. Iaconis, *Quantum state complexity in computationally tractable quantum circuits*, PRX Quantum **2**, 010329 (2021).
 - [19] M. A. Nielsen and I. L. Chuang, *Quantum Computation and Quantum Information*, Cambridge University Press (2000).

-
- [20] F. G. S. L. Brandao, W. Chemissany, N. Hunter-Jones, R. Kueng, and J. Preskill, *Models of quantum complexity growth*, PRX Quantum **2**, 030316 (2021).
- [21] D. E. Parker, X. Cao, A. Avdoshkin, T. Scaffidi, and E. Altman, *A universal operator growth hypothesis*, Phys. Rev. **X9**, 041017 (2019).
- [22] K. Adhikari, S. Choudhury, and A. Roy, *Krylov complexity in quantum field theory*, Nucl. Phys. **B993**, 116263 (2023).
- [23] C. Liu, H. Tang, and H. Zhai, *Krylov complexity in open quantum systems*, Phys. Rev. Research **5**, 033085 (2023).
- [24] P. Caputa, J. M. Magan, and D. Patramanis, *Geometry of Krylov complexity*, Phys. Rev. Research **4**, 013041 (2022).
- [25] L. Lofgren, *Complexity of descriptions of systems: A foundational study*, Int. J. General Systems **3**, 197 (1977).
- [26] E. Olbrich, N. Bertschinger, N. Ay, and J. Jost, *How should complexity scale with system size?*, Eur. Phys. J. **B63**, 407 (2008).
- [27] V. Balasubramanian, P. Caputa, J. M. Magan, and Q. Wu, *Quantum chaos and the complexity of spread of states*, Phys. Rev. **D106**, 046007 (2022).
- [28] A. N. Kolmogorov, *Three approaches to the quantitative definition of information*, Int. J. Computer Mathematics **2**, 157 (1968).
- [29] J. Rissanen, *Modeling by the shortest data description*, Automatica **14**, 465 (1978).
- [30] J. Rissanen, *Stochastic complexity and modeling*, Ann. Stat. **14**, 1080 (1986).
- [31] M. A. Nielsen, *A geometric approach to quantum circuit lower bounds*, Quant. Inf. Comput. **6**, 213 (2006).
- [32] M. A. Nielsen, M. R. Dowling, M. Gu, and A. M. Doherty, *Quantum computation as geometry*, Science **311**, 1133 (2006).
- [33] M. R. Dowling and M. A. Nielsen, *The geometry of quantum computation*, Quant. Inf. Comput. **8**, 861 (2008).
- [34] C. Cafaro, L. Rossetti, and P. M. Alsing, *Complexity of quantum-mechanical evolutions from probability amplitudes*, Nucl. Phys. **B1010**, 116755 (2025).
- [35] C. Cafaro, E. Clements, and A. Alanazi, *Aspects of complexity in quantum evolutions on the Bloch sphere*, Eur. Phys. J. Plus **140**, 349 (2025).
- [36] R. Uzdin, U. Günther, S. Rahav, and N. Moiseyev, *Time-dependent Hamiltonians with 100% evolution speed efficiency*, J. Phys. A: Math. Theor. **45**, 415304 (2012).
- [37] C. Cafaro, S. Ray, and P. M. Alsing, *Geometric aspects of analog quantum search evolutions*, Phys. Rev. **A102**, 052607 (2020).
- [38] W. K. Wootters, *Statistical distance and Hilbert space*, Phys. Rev. **D23**, 357 (1981).
- [39] J. Samuel and R. Bhandari, *General setting for Berry's phase*, Phys. Rev. Lett. **60**, 2339 (1988).
- [40] P. M. Alsing, C. Cafaro, O. Luongo, C. Lupo, S. Mancini, and H. Quevedo, *Comparing metrics for mixed quantum states: Sjöqvist and Bures*, Phys. Rev. **A107**, 052411 (2023).
- [41] J. Alvarez-Vizoso, R. Arn, M. Kirby, C. Peterson, and B. Draper, *Geometry of curves in \mathbb{R}^n from the local singular value decomposition*, Lin. Algebra Appl. **571**, 180 (2019).
- [42] R. Millman and G. Parker, *Elements of Differential Geometry*, Prentice Hall, NY (1977).
- [43] I. S. Gradshteyn and I. M. Ryzhik, *Tables of Integrals, Series, and Products*, Academic Press (2000).
- [44] Kh. P. Gnatenko, H. P. Laba, and V. M. Tkachuk, *Geometric properties of evolutionary graph states and their detection on a quantum computer*, Phys. Lett. **A452**, 128434 (2022).
- [45] R. J. Banks et al., *Continuous-time quantum walks for MAX-CUT are hot*, Quantum **8**, 1254 (2024).
- [46] Kh. P. Gnatenko, *Entanglement of multi-qubit states representing directed networks and its detection with quantum computing*, Phys. Lett. **A521**, 129815 (2024).
- [47] Kh. P. Gnatenko, *Relation of curvature and torsion of weighted graph states with graph properties and its studies on a quantum computer*, Eur. Phys. J. Plus **140**, 241 (2025).
- [48] A. A. Nizami and A. W. Shrestha, *Krylov construction and complexity for driven quantum systems*, Phys. Rev. **E108**, 054222 (2023).
- [49] K. Takahashi and A. del Campo, *Krylov subspace methods for quantum dynamics with time-dependent generators*, Phys. Rev. Lett. **134**, 030401 (2025).
- [50] L. Landau, *A theory of energy transfer. II*, Phys. Z. Sowjet **2**, 46 (1932).
- [51] C. Zener, *Non-adiabatic crossing of energy levels*, Proc. R. Soc. **A137**, 696 (1932).
- [52] I. I. Rabi, *Space quantization in a gyrating magnetic field*, Phys. Rev. **51**, 652 (1937).
- [53] E. Barnes and S. Das Sarma, *Analytically solvable driven time-dependent two-level quantum systems*, Phys. Rev. Lett. **109**, 060401 (2012).
- [54] E. Barnes, *Analytically solvable two-level quantum systems and Landau-Zener interferometry*, Phys. Rev. **A88**, 013818 (2013).
- [55] A. Messina and H. Nakazato, *Analytically solvable Hamiltonians for quantum two-level systems and their dynamics*, J. Phys. A: Math and Theor. **47**, 44302 (2014).
- [56] R. Grimaudo, A. S. Magalhaes de Castro, H. Nakazato, and A. Messina, *Classes of exactly solvable generalized semi-classical Rabi systems*, Annalen der Physik **530**, 1800198 (2018).
- [57] E. R. Loubenets and C. Kading, *Specifying the unitary evolution of a qudit for a general nonstationary Hamiltonian via the generalized Gell-Mann representation*, Entropy **22**, 521 (2020).
- [58] A. S. Magalhaes de Castro, R. Grimaudo, D. Valenti, A. Migliore, H. Nakazato, and A. Messina, *Analytically solvable Hamiltonian in invariant subspaces*, Eur. Phys. J. Plus **138**, 766 (2023).
- [59] P. Kurzynski, *Multi-Bloch vector representation of the qutrit*, Quantum Inf. Comp. **11**, 361 (2011).
- [60] J. Xie et al., *Observing geometry of quantum states in a three-level system*, Phys. Rev. Lett. **125**, 150401 (2020).
- [61] C. Eltschka, M. Huber, S. Morelli, and J. Siewert, *The shape of higher-dimensional state space: Bloch-ball analog for a*

-
- gutrit*, *Quantum* **5**, 485 (2021).
- [62] O. Gamel, *Entangled Bloch spheres: Bloch matrix and two-qubit state space*, *Phys. Rev. A* **93**, 062320 (2016).
- [63] V. Balasubramanian, M. DeCross, A. Kar, and O. Parrikar, *Quantum complexity of time evolution with chaotic Hamiltonians*, *J. High Energ. Phys.* **2020**, 134 (2020).
- [64] T. Ali, A. Bhattacharyya, S. Shajidul Haque, E. H. Kim, N. Moynihan, and J. Murugan, *Chaos and complexity in quantum mechanics*, *Phys. Rev. D* **101**, 026021 (2020).
- [65] B. Craps, O. Evnin, and G. Pascuzzi, *A relation between Krylov and Nielsen complexity*, *Phys. Rev. Lett.* **132**, 160402 (2024).
- [66] S. E. Aguilar-Gutierrez and A. Rolph, *Krylov complexity is not a measure of distance between states or operators*, *Phys. Rev. D* **109**, L081701 (2024).
- [67] S. Seetharaman, C. Singh, and R. Nath, *Properties of Krylov state complexity in qubit dynamics*, *Phys. Rev. D* **111**, 076014 (2025).
- [68] S. PG, J. B. Kannan, R. Modak, and S. Aravinda, *Dependence of Krylov complexity saturation on the initial operator and state*, *Phys. Rev. E* **112**, L032203 (2025).
- [69] B. Craps, O. Evnin, and G. Pascuzzi, *Multiseed Krylov complexity*, *Phys. Rev. Lett.* **134**, 050402 (2025).

Appendix A: Complexity calculations

In this appendix, we provide some technical details on the derivations of Eqs. (51) and (56).

1. Exponential growth

In this first part of the appendix, we calculate the complexity of the quantum evolution in the exponential growth scenario. Specifically, we consider the case in which $\alpha(t) \stackrel{\text{def}}{=} \omega_0 t$, $\beta(t) \stackrel{\text{def}}{=} e^{\nu_0 t}$, and $0 \leq t \leq \pi/(2\omega_0)$. The state of the system at time t can be recast as,

$$\begin{aligned} |\psi(t)\rangle &= |\psi(\theta(t), \varphi(t))\rangle \\ &= \cos\left[\frac{\theta(t)}{2}\right] |0\rangle + e^{i\varphi(t)} \sin\left[\frac{\theta(t)}{2}\right] |1\rangle \\ &= \cos[\alpha(t)] |0\rangle + e^{i\beta(t)} \sin[\alpha(t)] |1\rangle. \end{aligned} \quad (\text{A1})$$

From Eq. (A1), we arrive at $\theta(t) = 2\alpha(t) = 2\omega_0 t$ and $\varphi(t) = \beta(t) = e^{\nu_0 t}$. Furthermore, since $0 \leq t \leq \pi/(2\omega_0)$, we also have $0 \leq \theta \leq \pi$ and $1 \leq \varphi \leq e^{\frac{\pi}{2}\frac{\nu_0}{\omega_0}}$. Given this temporal interval and these bounds on the parameters θ and φ , we can now proceed with the calculation of the instantaneous, accessed, and accessible volumes $V(t)$, \bar{V} , and V_{\max} , respectively. Recalling that volumes are positively defined, the instantaneous volume $V(t)$ becomes

$$V(t) = \left| \int_{\varphi(0)}^{\varphi(t)} \int_{\theta(0)}^{\theta(t)} \sqrt{g_{\text{FS}}(\theta, \varphi)} d\theta d\varphi \right| = \frac{[1 - \cos(2\omega_0 t)] (e^{\nu_0 t} - 1)}{4}. \quad (\text{A2})$$

From Eq. (A2), the accessed volume \bar{V} reduces to

$$\begin{aligned} \bar{V} &= \frac{2\omega_0}{\pi} \int_0^{\frac{\pi}{2\omega_0}} V(t) dt \\ &= \frac{2\omega_0}{\pi} \frac{1}{4} \int_0^{\frac{\pi}{2\omega_0}} [1 - \cos(2\omega_0 t)] (e^{\nu_0 t} - 1) dt \\ &= \frac{1}{4\pi} \int_0^{\pi} [1 - \cos(x)] \left(e^{\frac{1}{2}\frac{\nu_0}{\omega_0}x} - 1 \right) dx \\ &= \frac{1}{4\pi} \int_0^{\pi} [1 - \cos(x)] e^{\frac{1}{2}\frac{\nu_0}{\omega_0}x} dx - \frac{1}{4\pi} \int_0^{\pi} [1 - \cos(x)] dx \\ &= \frac{1}{4\pi} \int_0^{\pi} [1 - \cos(x)] e^{\frac{1}{2}\frac{\nu_0}{\omega_0}x} dx - \frac{1}{4}, \end{aligned} \quad (\text{A3})$$

where $x \stackrel{\text{def}}{=} 2\omega_0 t$. Finally, calculating the integral on the right-hand-side of Eq. (A3), we obtain

$$\bar{V} = \bar{V} \left(\frac{\nu_0}{\omega_0} \right) \stackrel{\text{def}}{=} \frac{\left[\left(\frac{\nu_0}{\omega_0} \right)^2 + 2 \right] e^{\frac{\pi}{2}\frac{\nu_0}{\omega_0}} - 2}{\pi \left(\frac{\nu_0}{\omega_0} \right) \left[\left(\frac{\nu_0}{\omega_0} \right)^2 + 4 \right]} - \frac{1}{4}. \quad (\text{A4})$$

Lastly, the accessible volume V_{\max} reduces to

$$\begin{aligned} V_{\max} &= \left| \int_{\varphi_{\min}}^{\varphi_{\max}} \int_{\theta_{\min}}^{\theta_{\max}} \sqrt{g_{\text{FS}}(\theta, \varphi)} d\theta d\varphi \right| \\ &= \left| \int_1^{e^{\frac{\pi}{2}\frac{\nu_0}{\omega_0}}} \int_0^{\pi} \sqrt{g_{\text{FS}}(\theta, \varphi)} d\theta d\varphi \right| \\ &= \frac{1}{4} \left| \left(\int_0^{\pi} \sin(\theta) d\theta \right) \left(\int_1^{e^{\frac{\pi}{2}\frac{\nu_0}{\omega_0}}} d\varphi \right) \right| \\ &= \frac{e^{\frac{\pi}{2}\frac{\nu_0}{\omega_0}} - 1}{2}, \end{aligned} \quad (\text{A5})$$

that is,

$$V_{\max} = V_{\max} \left(\frac{\nu_0}{\omega_0} \right) \stackrel{\text{def}}{=} \frac{e^{\frac{\pi}{2} \frac{\nu_0}{\omega_0}} - 1}{2}. \quad (\text{A6})$$

Finally, combining Eqs. (A4) and (A6), we arrive at the complexity of this particular quantum evolution. We get,

$$C = \frac{V_{\max} - V}{V_{\max}} = \frac{\frac{e^{\frac{\pi}{2} \frac{\nu_0}{\omega_0}} - 1}{2} - \left(\frac{\left[\left(\frac{\nu_0}{\omega_0} \right)^2 + 2 \right] e^{\frac{\pi}{2} \frac{\nu_0}{\omega_0}} - 2}{\pi \left(\frac{\nu_0}{\omega_0} \right) \left[\left(\frac{\nu_0}{\omega_0} \right)^2 + 4 \right]} - \frac{1}{4} \right)}{\frac{e^{\frac{\pi}{2} \frac{\nu_0}{\omega_0}} - 1}{2}}, \quad (\text{A7})$$

that is, after some algebraic manipulations,

$$C = C \left(\frac{\nu_0}{\omega_0} \right) \stackrel{\text{def}}{=} \frac{\left[2\pi \left(\frac{\nu_0}{\omega_0} \right)^3 - 4 \left(\frac{\nu_0}{\omega_0} \right)^2 + 8\pi \frac{\nu_0}{\omega_0} - 8 \right] e^{\frac{\pi}{2} \frac{\nu_0}{\omega_0}} - \left[\pi \left(\frac{\nu_0}{\omega_0} \right)^3 + 4\pi \frac{\nu_0}{\omega_0} - 8 \right]}{\left[2\pi \left(\frac{\nu_0}{\omega_0} \right)^3 + 8\pi \frac{\nu_0}{\omega_0} \right] e^{\frac{\pi}{2} \frac{\nu_0}{\omega_0}} - \left[2\pi \left(\frac{\nu_0}{\omega_0} \right)^3 + 8\pi \frac{\nu_0}{\omega_0} \right]}. \quad (\text{A8})$$

Note that setting $\xi \stackrel{\text{def}}{=} \nu_0/\omega_0$, we have

$$\lim_{\xi \rightarrow \infty} C(\xi) = \lim_{\xi \rightarrow \infty} \frac{(2\pi\xi^3 - 4\xi^2 + 8\pi\xi - 8) e^{\frac{\pi}{2}\xi} - (\pi\xi^3 + 4\pi\xi - 8)}{(2\pi\xi^3 + 8\pi\xi) e^{\frac{\pi}{2}\xi} - (2\pi\xi^3 + 8\pi\xi)} = 1, \quad (\text{A9})$$

and,

$$\lim_{\xi \rightarrow 0} C(\xi) = \lim_{\xi \rightarrow 0} \frac{(2\pi\xi^3 - 4\xi^2 + 8\pi\xi - 8) e^{\frac{\pi}{2}\xi} - (\pi\xi^3 + 4\pi\xi - 8)}{(2\pi\xi^3 + 8\pi\xi) e^{\frac{\pi}{2}\xi} - (2\pi\xi^3 + 8\pi\xi)} = \frac{3\pi^2 - 4}{4\pi^2} \sim 0.65. \quad (\text{A10})$$

Therefore, in the limit of $\nu_0/\omega_0 \rightarrow 0$ of Eq. (A10), the limiting value of the complexity in the exponential growth case reduces to the one we obtained in the linear growth case. Indeed, keeping in mind the specifics of the linear growth case, this behavior can be explained by observing that when $\nu_0/\omega_0 \rightarrow 0$, the exponential growth case is characterized by $\varphi(t) \approx 1 + \nu_0 t$ with $1 \leq \varphi(t) \lesssim 1 + (\pi/2)(\nu_0/\omega_0)$. Moreover, when $\nu_0/\omega_0 \rightarrow \infty$ as in Eq. (A9), $\bar{V} \approx (\nu_0/\omega_0)^{-1} e^{\frac{\pi}{2} \frac{\nu_0}{\omega_0}}$, and $V_{\max} \approx e^{\frac{\pi}{2} \frac{\nu_0}{\omega_0}}$. Therefore, $\bar{V}/V_{\max} \approx (\nu_0/\omega_0)^{-1} \rightarrow 0$ as ν_0/ω_0 diverges. This type of behavior specifies a maximal complexity scenario in which C approaches its maximal value one.

2. Exponential decay

In this second part of the appendix, we evaluate the complexity of the quantum evolution in the exponential decay case. Specifically, we assume to consider the case where $\alpha(t) \stackrel{\text{def}}{=} \omega_0 t$, $\beta(t) \stackrel{\text{def}}{=} e^{-\nu_0 t}$, and $0 \leq t \leq \pi/(2\omega_0)$. The state of the system at time t can be written as,

$$\begin{aligned} |\psi(t)\rangle &= |\psi(\theta(t), \varphi(t))\rangle \\ &= \cos \left[\frac{\theta(t)}{2} \right] |0\rangle + e^{i\varphi(t)} \sin \left[\frac{\theta(t)}{2} \right] |1\rangle \\ &= \cos [\alpha(t)] |0\rangle + e^{i\beta(t)} \sin [\alpha(t)] |1\rangle. \end{aligned} \quad (\text{A11})$$

From Eq. (A11), we get $\theta(t) = 2\alpha(t) = 2\omega_0 t$ and $\varphi(t) = \beta(t) = e^{-\nu_0 t}$. Furthermore, since $0 \leq t \leq \pi/(2\omega_0)$, we also have $0 \leq \theta \leq \pi$ and $e^{-\frac{\pi}{2} \frac{\nu_0}{\omega_0}} \leq \varphi \leq 1$. Given this temporal interval and these bounds on the parameters θ and φ , we can now proceed with the computation of the instantaneous, accessed, and accessible volumes $V(t)$, \bar{V} , and V_{\max} , respectively. Recalling that volumes are positive quantities, the instantaneous volume $V(t)$ becomes

$$V(t) = \left| \int_{\varphi(0)}^{\varphi(t)} \int_{\theta(0)}^{\theta(t)} \sqrt{g_{\text{FS}}(\theta, \varphi)} d\theta d\varphi \right| = \frac{[1 - \cos(2\omega_0 t)] (1 - e^{-\nu_0 t})}{4}. \quad (\text{A12})$$

From Eq. (A12), the accessed volume \bar{V} is given by

$$\begin{aligned}
\bar{V} &= \frac{2\omega_0}{\pi} \int_0^{\frac{\pi}{2\omega_0}} V(t) dt \\
&= \frac{2\omega_0}{\pi} \frac{1}{4} \int_0^{\frac{\pi}{2\omega_0}} [1 - \cos(2\omega_0 t)] (1 - e^{-\nu_0 t}) dt \\
&= \frac{1}{4\pi} \int_0^{\pi} [1 - \cos(x)] \left(1 - e^{-\frac{1}{2}\frac{\nu_0}{\omega_0}x}\right) dx \\
&= \frac{1}{4\pi} \int_0^{\pi} [1 - \cos(x)] dx - \frac{1}{4\pi} \int_0^{\pi} [1 - \cos(x)] e^{-\frac{1}{2}\frac{\nu_0}{\omega_0}x} dx \\
&= \frac{1}{4} - \frac{1}{4\pi} \int_0^{\pi} [1 - \cos(x)] e^{-\frac{1}{2}\frac{\nu_0}{\omega_0}x} dx,
\end{aligned} \tag{A13}$$

where $x \stackrel{\text{def}}{=} 2\omega_0 t$. Finally, evaluating the integral on the right-hand-side of Eq. (A13), we get

$$\bar{V} = \bar{V} \left(\frac{\nu_0}{\omega_0} \right) \stackrel{\text{def}}{=} \frac{1}{4} - \frac{2 - \left[\left(\frac{\nu_0}{\omega_0} \right)^2 + 2 \right] e^{-\frac{\pi}{2}\frac{\nu_0}{\omega_0}}}{\pi \left(\frac{\nu_0}{\omega_0} \right) \left[\left(\frac{\nu_0}{\omega_0} \right)^2 + 4 \right]}. \tag{A14}$$

Ultimately, the accessible volume V_{\max} becomes

$$\begin{aligned}
V_{\max} &= \left| \int_{\varphi_{\min}}^{\varphi_{\max}} \int_{\theta_{\min}}^{\theta_{\max}} \sqrt{g_{\text{FS}}(\theta, \varphi)} d\theta d\varphi \right| \\
&= \left| \int_{e^{-\frac{\pi}{2}\frac{\nu_0}{\omega_0}}}^1 \int_0^{\pi} \sqrt{g_{\text{FS}}(\theta, \varphi)} d\theta d\varphi \right| \\
&= \frac{1}{4} \left| \left(\int_0^{\pi} \sin(\theta) d\theta \right) \left(\int_{e^{-\frac{\pi}{2}\frac{\nu_0}{\omega_0}}}^1 d\varphi \right) \right| \\
&= \frac{1 - e^{-\frac{\pi}{2}\frac{\nu_0}{\omega_0}}}{2},
\end{aligned} \tag{A15}$$

that is,

$$V_{\max} = V_{\max} \left(\frac{\nu_0}{\omega_0} \right) \stackrel{\text{def}}{=} \frac{1 - e^{-\frac{\pi}{2}\frac{\nu_0}{\omega_0}}}{2}. \tag{A16}$$

Finally, making use of Eqs. (A14) and (A16), we obtain the complexity of this particular quantum evolution. We arrive at

$$C = \frac{V_{\max} - V}{V_{\max}} = \frac{\frac{1 - e^{-\frac{\pi}{2}\frac{\nu_0}{\omega_0}}}{2} - \left(\frac{1}{4} - \frac{2 - \left[\left(\frac{\nu_0}{\omega_0} \right)^2 + 2 \right] e^{-\frac{\pi}{2}\frac{\nu_0}{\omega_0}}}{\pi \left(\frac{\nu_0}{\omega_0} \right) \left[\left(\frac{\nu_0}{\omega_0} \right)^2 + 4 \right]} \right)}{\frac{1 - e^{-\frac{\pi}{2}\frac{\nu_0}{\omega_0}}}{2}}, \tag{A17}$$

that is, after some algebraic manipulations,

$$C = C \left(\frac{\nu_0}{\omega_0} \right) \stackrel{\text{def}}{=} \frac{\left[\pi \left(\frac{\nu_0}{\omega_0} \right)^3 + 4\pi \left(\frac{\nu_0}{\omega_0} \right) + 8 \right] e^{\frac{\pi}{2}\frac{\nu_0}{\omega_0}} - \left[2\pi \left(\frac{\nu_0}{\omega_0} \right)^3 + 4 \left(\frac{\nu_0}{\omega_0} \right)^2 + 8\pi \left(\frac{\nu_0}{\omega_0} \right) + 8 \right]}{\left[2\pi \left(\frac{\nu_0}{\omega_0} \right)^3 + 8\pi \left(\frac{\nu_0}{\omega_0} \right) \right] e^{\frac{\pi}{2}\frac{\nu_0}{\omega_0}} - \left[2\pi \left(\frac{\nu_0}{\omega_0} \right)^3 + 8\pi \left(\frac{\nu_0}{\omega_0} \right) \right]}. \tag{A18}$$

Observe that putting $\xi \stackrel{\text{def}}{=} \nu_0/\omega_0$, we obtain

$$\lim_{\xi \rightarrow \infty} C(\xi) = \lim_{\xi \rightarrow \infty} \frac{(\pi\xi^3 + 4\pi\xi + 8) e^{\frac{\pi}{2}\xi} - (2\pi\xi^3 + 4\xi^2 + 8\pi\xi + 8)}{(2\pi\xi^3 + 8\pi\xi) e^{\frac{\pi}{2}\xi} - (2\pi\xi^3 + 8\pi\xi)} = \frac{1}{2}, \tag{A19}$$

and,

$$\lim_{\xi \rightarrow 0} C(\xi) = \lim_{\xi \rightarrow 0} \frac{(2\pi\xi^3 - 4\xi^2 + 8\pi\xi - 8) e^{\frac{\pi}{2}\xi} - (\pi\xi^3 + 4\pi\xi - 8)}{(2\pi\xi^3 + 8\pi\xi) e^{\frac{\pi}{2}\xi} - (2\pi\xi^3 + 8\pi\xi)} = \frac{3\pi^2 - 4}{4\pi^2} \sim 0.65. \quad (\text{A20})$$

Therefore, in the limit of $\nu_0/\omega_0 \rightarrow 0$ of Eq. (A20), the limiting value of the complexity in the exponential decay case equals the one we obtained in the linear growth case. Indeed, taking into consideration the details of the linear growth case, this behavior can be grasped by noting that when $\nu_0/\omega_0 \rightarrow 0$, the exponential decay case is specified by $\varphi(t) \approx 1 - \nu_0 t$ with $1 - (\pi/2)(\nu_0/\omega_0) \leq \varphi(t) \lesssim 1$. Moreover, when $\nu_0/\omega_0 \rightarrow \infty$ as in Eq. (A19), $\varphi(t)$ becomes constant and we recover the same complexity value calculated in the no growth case.

With these observations and with the derivations of Eqs. (A8) and (A18), we end this appendix.